

SPECTROSCOPY OF JAROSITE MINERALS, AND IMPLICATIONS
FOR THE MINERALOGY OF MARS

YARROW ROTHSTEIN

Mount Holyoke College

Advisors:

Professor M. Darby Dyar

Department of Astronomy, Mount Holyoke College

&

Professor Catrina Hamilton

Department of Astronomy, Mount Holyoke College and University of Massachusetts

&

Professor Peter Berek

Department of English, Mount Holyoke College

Presented to the Department of Astronomy

May 2006

ACKNOWLEDGMENTS

- Darby Dyar- for being a supportive mentor and allowing me to do undergraduate research with her for four years. She was always ready to help whenever I needed an extra pair of eyes or hands for my thesis.
- George Brophy- for making the synthetic samples that I used for my thesis.
- Thesis Committee (Darby Dyar, Catrina Hamilton, and Peter Berek) - for reviewing my thesis and giving direction as how to make it better.
- My family- for always supporting me in my scientific endeavors.
- My friends- for being there when writing my thesis was taking over my life and helping me realize that it would be completed eventually.

TABLE OF CONTENTS	
ACKNOWLEDGMENTS	ii
LIST OF FIGURES	iiv
TABLE OF TABLES	vi
ABSTRACT	vii
INTRODUCTION	1
BACKGROUND	10
Jarosite Chemistry	10
FTIR Spectroscopy	12
The Technique of Mössbauer Spectroscopy	27
MÖSSBAUER STUDIES OF JAROSITE AND ALUNITE	46
METHODS	49
Infrared Methods	50
Mössbauer methods	50
RESULTS AND DISCUSSION	57
Mössbauer	57
Infrared	71
CONCLUSIONS	76
REFERENCES	80

LIST OF FIGURES

Figure 1.1: Jarosite	2
Figure 1.2: Map of Meridian Planum landing site	4
Figure 1.3: The MERs Mössbauer spectrometer	6
Figure 1.4: APXS spectrometer mounted on to MER	7
Figure 1.5: Mini-TES on MER	8
Figure 1.6: Pancam on MER	9
Figure 2.1: Jarosite crystal figure	11
Figure 2.2: Bending and stretching in IR Spectroscopy	14
Figure 2.3: Diagram of particles receiving energy	29
Figure 2.4: Illustration of Mössbauer process	32
Figure 2.5: Diagram of the various paths an electron	33
Figure 2.6: Diagram of the parameters of Mössbauer	35
Figure 2.7: Isomer shift versus quadrupole splitting	36
Figure 3.1: Jarosite fit with one doublet	53
Figure 3.2: Jarosite fit with two doublets	54
Figure 3.3: Jarosite fit with three doublets	55
Figure 3.4: Jarosite fit with three doublets and a sextet	56
Figure 4.1: Isomer shift and quadrupole splitting of doublets	61
Figure 4.2: Graphs with current and previous studies	62
Figure 4.3: One doublet fits	66
Figure 4.4: MER Mössbauer data	67

Figure 4.5: IR spectra from 900 to 6000 nm	71
Figure 4.6: IR spectra from 900 to 2700 nm	72
Figure 4.7: IR spectra of three different grain sizes	74
Figure 4.8: Composition changes in IR	75

TABLE OF TABLES

Table 2.1: Mineral in the Jarosite and Alunite subgroups	12
Table 2.2: IR jarosite and alunite data by Adler, H.H., et al. (1965)	19
Table 2.3: IR jarosite and alunite data by Ross, D.S. (1974)	19
Table 2.4: IR jarosite data by Powers (1975)	20
Table 2.5: IR jarosite data from Serna et al. (1986)	21
Table 2.6: IR jarosite data by Sasaki (1998)	23
Table 2.7: IR jarosite data by Music (2000)	24
Table 2.8: IR jarosite data by Bishop (2005)	25
Table 2.9: Mössbauer parameters of jarosite	48
Table 3.2: Jarosite 6B fit with an assortment of different parameters	51
Table 4.1: Mössbauer table of the two typical jarosite doublets	59
Table 4.2: Mössbauer data for jarosite spectra fit with only one peak	64
Table 4.3: The refit Mars Mössbauer data's possible jarosite peak	68
Table 4.4: Low temperature jarosite Mössbauer parameters	69
Table 4.5: Mössbauer parameters of sulfates at room temperature	70
Table 4.6: Jarosite peak values in nm	73

ABSTRACT

The Mars Exploration Rover Mössbauer spectroscopy team identified jarosite, a sulfate which forms in the presence of water, in spectra of a layered outcrop in Meridiani Planum (Klingelhöfer et al. 2004). They made this assignment based on a doublet with quadrupole splitting of ~ 1.22 mm/s at $T=200-280$ K that was assigned to either K^+ or Na^+ jarosite with the possibility of some Al substituting for Fe in octahedral sites. In order to further characterize this jarosite at Meridiani and search for jarosite elsewhere, careful spectroscopic characterization of the Mössbauer parameters of jarosite over a range of compositions and temperatures is needed, which is the goal of this study. The jarosite group has the formula $AM_3(SO_4)_2(OH)_6$, where A is usually a monovalent cation (K^+ and Na^+ are most common, although Pb^+ , Ag^+ , NH_4^+ and H_3O^+ are also observed). M is primarily Fe^{3+} for jarosite, Al^{3+} for alunite or another trivalent cation. The structure is composed of SO_4^{2-} tetrahedral and $MO_2(OH)_4$ octahedra, both somewhat distorted and each forming a layer in the a direction. Each SO_4^{2-} tetrahedron has one O bound to Al or Fe, producing a symmetry of $C3v$ instead of Td .

The jarosite samples used in this study were synthesized by Brophy (Brophy, 1965) and were generously provided to us by him. They represent a series of 17 compositions in which the values of potassium (K), sodium (Na), and hydronium (H_3O) all vary. Mössbauer spectra of all samples were acquired at room temperature; sample #2 was also measured over a range of 16 temperatures from 12-295K at low He gas pressure. A source of 100-70 mCi ^{57}Co in Rh was used on a WEB Research Co. model W100 spectrometer equipped with a Janus closedcycle He refrigerator. Run times ranged from 1-12 hours; results were calibrated against α -Fe foil.

At low K contents, Na and H₃O⁺ were co-varied, so the trends are not clear. These data contrast with the much older work, who suggested that the QS values of jarosite are *negatively* correlated with K contents. However, those earlier studies used Lorentzian doublets rather than QSD's, employed natural samples that were part of mixtures of minerals, and/or had far fewer compositions represented. Our multi-temperature Mössbauer spectra show that magnetic ordering in jarosite with a composition of K_{0.74}Na_{0.02}(H₃O)_{0.24} occurs at 90 K.

The NIR spectrum of K-jarosite exhibits an OH stretching band at 1.47 μm, an OH stretch + 2 bend combination doublet at 1.849 and 1.864 μm, plus an OH stretch + bend combination triplet at 2.215, 2.265, and 2.300 μm and additional OH and SO₄ combination features near 2.40, 2.46, 2.50, 2.60 and 2.62 μm. H₃O and Na-jarosite spectra exhibit broader features and the doublet is less resolvable. The spectrum of Na-jarosite contains a band at 1.48 μm, a broad asymmetric band near 1.85 μm and a triplet near 2.235, 2.275, and 2.310 μm, plus additional features near 2.42, 2.47, 2.52, 2.62 and 2.64 μm.

INTRODUCTION

The goal of this thesis is to characterize and interpret the spectroscopic characteristics of the alunite mineral group, with emphasis on the Fe^{3+} -bearing jarosite species within this group such as jarosite, $\text{KFe}_3(\text{SO}_4)_2(\text{OH})_6$. The alunite-jarosite group was chosen to be the main focus of this thesis because of its recent “discovery” based on interpretation of the Mössbauer data from the Mars Exploration Rovers (Klingelhöfer et al., 2004). This result was exciting because jarosite only forms in the presence of water. If it is possible to confirm that the mineral identified is indeed jarosite, it can then be concluded that there was water on the surface of Mars when the rocks formed. This would be very important because one of the main goals of the mission to Mars was to try to confirm if there ever had been water present on the Martian surface

On Earth, jarosite forms in one of four different types of occurrences. The first is in oxidized sulfate sections of ore deposits or in pyrite-rich rocks such as coal. In these parageneses, jarosite often forms as a coating on the other Fe sulfate minerals. The second is in clays, either as small, hard lumps called nodules or spread diffusely through other clay minerals. This is thought to occur because the oxidation of the pyrite contained in the clay provides the iron and sulfate, while the acid is drawn out of the clay and provides the alkalis. The third

occurrence is in acid soils, where the molecules that make up the soil are either able to give a hydrogen ion or want to accept a pair of electrons. Acidic substances have a pH level, which is a measure of the hydrogen-ion concentration, of less than 7. There are many places around the world where the soil has a pH of 3 or 4; when this occurs in marine sediments, it is then likely that the soil also contains pyrite, resulting in a yellow soil (Warshaw 1956). The fourth is in hydrothermal deposits, where jarosite is a hypogene mineral, meaning it is formed under or found below the earth's surface. Examples of this are found at hot-spring deposits in Yellowstone National Park (Allen and Day 1935) and in Japan (Kinoshitea et al., 1955, Saito, 1962), as well as Indonesia (Zelenov and Tkachenko 1970). Figure 1.1 shows a typical hand sample of jarosite.

Figure 1.1: Jarosite

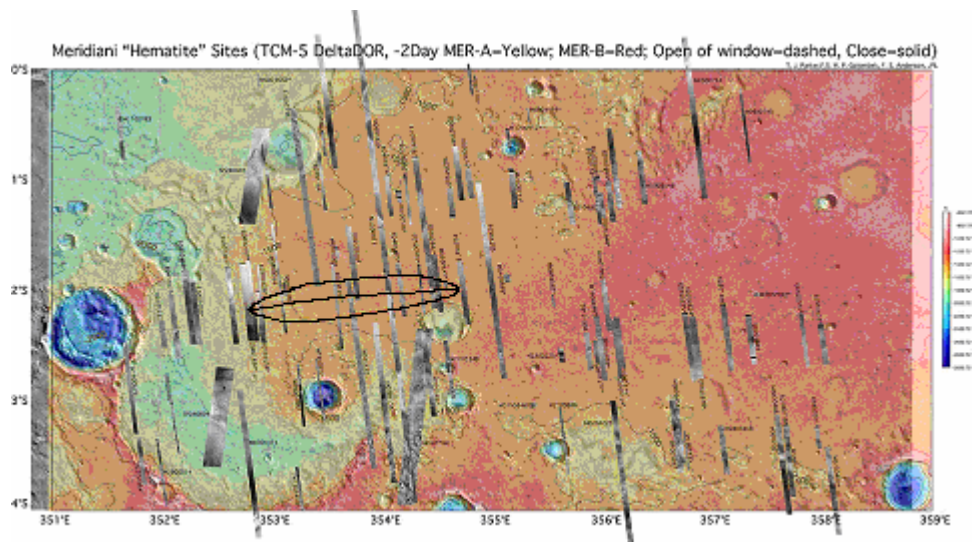


Conditions for formation of jarosite on Mars may exist or have existed there in the past. Just as on Earth, on Mars jarosite may form when acidic conditions existed along with oxidized iron sulfides and the two were then weathered. The minerals probably present on Mars are described by Burns (1987,

1988) and his predictions are supported by the mineralogy of the Martian meteorites (e.g. Nakhla and basaltic shergottites (McSween, 1985)). Burns and Fisher (1990) also proposed a scenario that might have occurred on Mars, where the ground had been weathered by acid water that would turn pyrrhotite into pyrite and then into goethite and jarosite. The jarosite could then not be further altered (Bishop et al., 2005). As a result of this previous work, it was predicted that jarosite would be a likely mineral to be found by the exploration rovers on Mars, provided the appropriate instrumentation was on-board.

In 2003, NASA launched the pair of Mars Exploration Rovers which landed on Mars 3 weeks apart in January of 2004: Spirit and Opportunity. The chosen landing sites were at Gusev Crater and Meridiani Planum, respectively. These sites were chosen because satellite data suggested that water might possibly have previously existed there. Gusev Crater was thought to have had a lake in its crater, while spectroscopic data had placed hematite, also a mineral forming in water, in Meridiani Planum. Figure 1.2 is a picture of Meridiani Planum with the landing site enclosed by the ellipse.

Figure 1.2: Map of Meridiani Planum landing site



Picture from: http://marsoweb.nas.nasa.gov/landingsites/mer2003/topsites/final/Hematite/maps/Hematite_small.jpg

The sites were chosen because of their scientific interest, but also because they seemed to be relatively safe areas on which to land. Meridiani Planum was chosen as the safer choice, since it is flatter and therefore the rover had more chance of surviving the landing in working condition. The site is located by the Martian equator and was also chosen because it had several different types of geological features. The Gusev Crater is more to the south than Meridiani Planum and is also almost on the opposite side of the planet. It was chosen as the slightly more dangerous landing site, but it was also seen as a better bet for accomplishing the mission goals of finding water because previous data seemed to indicate it might be a dried up lake bed.

The rovers had several scientific goals, focusing on determining if there had been water on the surface of Mars by characterizing the minerals found and the geological processes that formed the surface. Secondary goals were to perform tests that would serve as calibrations for spectroscopic data that were not obtained on the ground.

The rovers carried four cameras, the hazard avoiding cameras (Hazcam), the navigation cameras (Navcam) the panoramic cameras (PanCam) and the microscopic imager (MI), three spectrometers, the miniature thermal emission spectrometer (Mini-TES), the Mössbauer spectrometer (MB), and the alpha particle x-ray spectrometer (APXS), and two aiding tools, the rock abrasion tool (RAT) and the magnet array. Three of these are instruments related to the current work: the PanCam (visible region spectra), the TES (IR), and the Mössbauer. These three spectrometers were used to prove the existence of jarosite on Mars, as follows.

The Mössbauer spectrometer is a tool to help determine the valence state and the site occupancy of iron in a mineral structure. The instrument cannot be used by itself to obtain a definite identification because many minerals have similar valences (Fe^0 , Fe^{2+} , Fe^{3+}) and crystallographic sites (tetrahedral and octahedran), so they will have similar Mössbauer parameters. The Mössbauer

spectroscopy team claimed that in one of their spectra from an outcrop in Meridiani Planum, they found jarosite (Klingelhöfer et al., 2004). They made this assignment because the spectra contained one doublet with a parameter that matched jarosite in their database, which was a collection of Mössbauer data published in the literature and formatted for use in searches by the Mössbauer Effect Data Center (<http://orgs.unca.edu/medc/>). Figure 1.3 is a picture of the Mössbauer spectrometer used on the Mars Rovers.

Figure 1.3: The MERs Mössbauer spectrometer



Picture from: http://marsrovers.jpl.nasa.gov/mission/spacecraft_instru_mossbr.html

The Alpha Particle-X-Ray Spectrometer (APXS) is an instrument that determines the elemental compositions of rocks and minerals using alpha particles and x-rays. It discovered a large percentage of sulfur, around 25% in an outcrop, but only a small quantity of S, about 1/5 of that in the Meridiani soil, where the jarosite was claimed to have been found. Figure 1.4 is a picture of the APXS that was attached to the robotic arm of the MERs.

Figure 1.4: APXS spectrometer mounted on to MER



Picture from: http://marsrovers.jpl.nasa.gov/mission/spacecraft_instru_apxs.html

The Miniature Thermal Emission Spectrometer (Mini-TES) (Christensen, et al., 2004) is a Michelson interferometer that acquires infrared spectra from 339 to 1997 cm^{-1} . Its data from the Meridiani site showed that 15 to 35% of the outcrops were sulfate; the best fits were provided by Mg^{2+} and Ca^{2+} rich sulfates. The Mini-TES might have located jarosite, but because the amount was never above 5% of the total spectra it is hard to definitively state if the mineral was there. However, using other measurements of iron from the other MER instruments, the science team thinks that jarosite might be as much as 10% by weight of the outcrop. However, they also decided that the outcrop couldn't be made of jarosite alone. There had to be other sulfates present because there was too much sulfur and not enough iron for the mineral to just be jarosite

(Christensen, et al., 2004). Figure 2.5 is a picture of the Mini-TES that was used by the MERS on Mars.

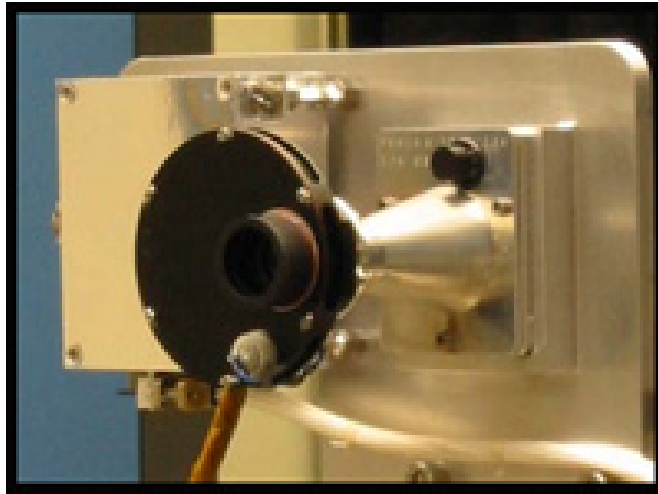
Figure 1.5: Mini-TES on MER



Picture from: http://marsrovers.jpl.nasa.gov/mission/spacecraft_instru_minites.html

The Pancam is one of the cameras on the Meridiani Planum MER that took high resolution multispectral images of the surface of Mars. The Pancam spectra of the outcrops in different craters indicated nanophase ferric iron, and citing the other science teams' results and conclusions, hypothesized that the ferric iron was jarosite. The dark sand had a strong band at 530 nm and a weaker band at 900 to 950 nm, which also point to ferric iron, however this was assigned other sulfates, such as schwertmannite, ferrihydrite or disordered goethite (Bell et al., 2004). Figure 1.6 is an image of the Pancam used on the MERs.

Figure 1.6: Pancam on MER



Picture from: http://marsrovers.jpl.nasa.gov/mission/spacecraft_instru_pancam.html

The main goal of this thesis is to use spectroscopy to examine synthetic samples that are definitely known to be jarosite. These data provide a basis for comparison with the MER data, making it is possible to decide whether or not the science team made a correct interpretation.

BACKGROUND

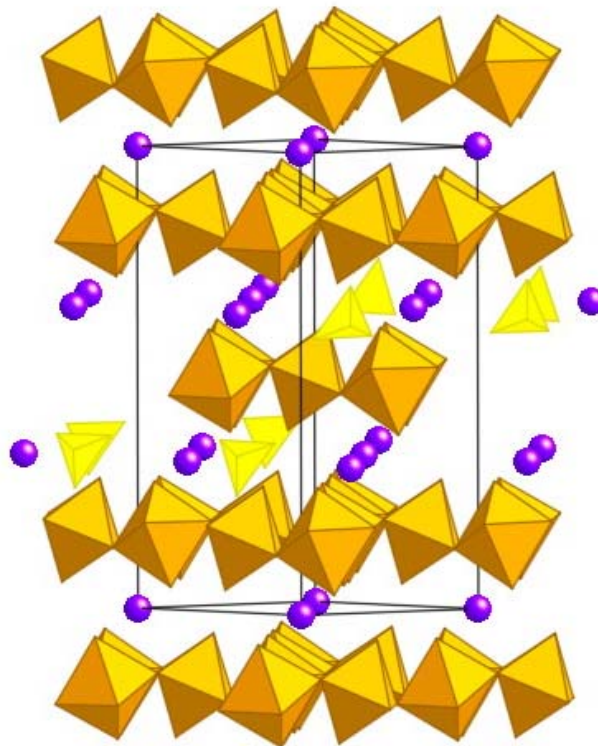
Jarosite Chemistry

Jarosite is a mineral species that is a member of the alunite supergroup, which contains 16 minerals. The general formula for the supergroup is $DG_3(TO_4)_2(OH,H_2O)_6$, where D is a cation in 9-fold coordination with oxygen, G with 6 oxygens, and T with 4 oxygens (Smith et al., 1998).

The D cations can be K (potassium), Na (sodium), H_3O (hydronium), NH_4 (ammonia), Ag (silver), Pb (lead), Tl (thallium), Ca (calcium), or Ba (barium). There are five elements that are found in the T position: S (sulfur), P (phosphate), V (vanadium), Si (silicon), or As (arsenic). Smith et al. (1998), like Dutrizac and Jambor (2000), use the TO_4 compound to separate the minerals into the crandallite and arsenocrandallite subgroups. Of these, the S-bearing subgroups are then further distinguished by the composition of G, which will usually be occupied by Fe^{3+} or Al^{3+} with minor amounts of Cu (copper) sometimes present. If the Fe^{3+} content is greater than the Al^{3+} content, the mineral belongs to the jarosite subgroup. If Al^{3+} is greater than Fe^{3+} , then the mineral is classified in the alunite subgroup.

The minerals in the alunite supergroup sometimes crystallize into characteristic crystal forms that are indicative of their internal atomic structure. The crystals are usually small and rare, being found more often as films, crusts or earthy masses. Crystals are usually rhombohedral in shape, which are composed of two trigonal pyramids stacked on top of each other, as seen in Figure 2.1. The orange structures represent either the iron or sulfur surrounded by oxygen and hydrogen. The purple circles are K, Na, or H₃O and the yellow triangles are the sulfur surrounded by oxygen.

Figure 2.1: Jarosite crystal figure



In the alunite and jarosite subgroups, the Al^{3+} or Fe^{3+} (G) ions are as far apart from each other and the sulfur atoms as is allowed by the structure. Each Al or Fe atom is surrounded by four OH groups and two oxygens that are part of two different SO_4 (T) groups, forming an octahedron. Each sulfur is found in a fourfold coordination with three equidistant oxygen atoms and one additional oxygen atom that is closer to the sulfur than the other three. The D cations are surrounded with oxygens from six different SO_4 groups.

Table 2.1: Mineral in the Jarosite and Alunite subgroups

jarosite	jarosite	$\text{KFe}_3(\text{SO}_4)_2(\text{OH})_6$
	natrojarosite	$\text{NaFe}_3(\text{SO}_4)_2(\text{OH})_6$
	ammoniojarosite	$(\text{NH}_4)\text{Fe}_3(\text{SO}_4)_2(\text{OH})_6$
	hydronium jarosite	$(\text{H}_3\text{O})\text{Fe}_3(\text{SO}_4)_2(\text{OH})_6$
	argentojarosite	$\text{AgFe}_3(\text{SO}_4)_2(\text{OH})_6$
	dorallcharite	$\text{TlFe}_3(\text{SO}_4)_2(\text{OH})_6$
	beaverite	$\text{Pb}(\text{Fe,Cu})_3(\text{SO}_4)_2(\text{OH})_6$
	plumbojarosite	$\text{PbFe}_6(\text{SO}_4)_4(\text{OH})_{12}$
Alunite	alunite	$\text{KAl}_3(\text{SO}_4)_2(\text{OH})_6$
	natroalunite	$\text{NaAl}_3(\text{SO}_4)_2(\text{OH})_6$
	ammonioalunite	$(\text{NH}_4)\text{Al}_3(\text{SO}_4)_2(\text{OH})_6$
	schlossmacherite	$(\text{H}_3\text{O})\text{Al}_3(\text{SO}_4)_2(\text{OH})_6$
	osarizawaite	$\text{Pb}(\text{Al,Cu})_3(\text{SO}_4)_2(\text{OH,H}_2\text{O})_6$
	minamiite	$(\text{Na,Ca})_2\text{Al}_6(\text{SO}_4)_4(\text{OH})_{12}$
	huangite	$\text{CaAl}_6(\text{SO}_4)_4(\text{OH})_{12}$
	walthierite	$\text{BaAl}_6(\text{SO}_4)_4(\text{OH})_{12}$

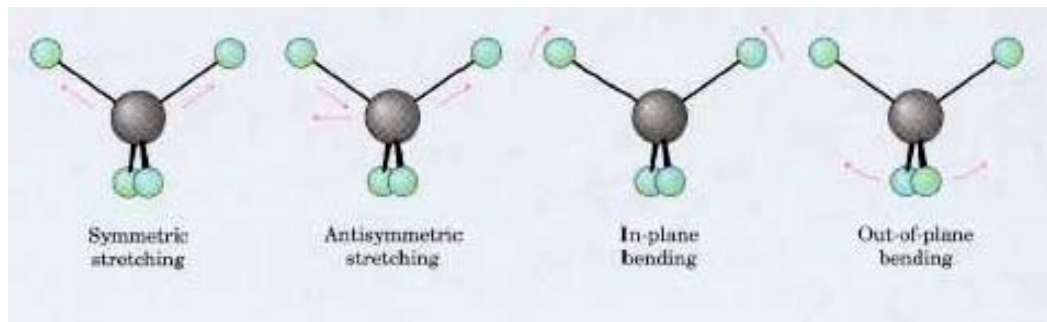
It is worth noting that there are other minerals in the alunite supergroup with this structure. The minerals in the crandallite group (e.g., $\text{Al}_3(\text{PO}_4)_2(\text{OH})_5 \cdot \text{H}_2\text{O}$) contain the PO_4 compound, while arsenocrandallite

$((\text{Ca,Sr})\text{Al}_3[(\text{As,P})\text{O}_4]_2(\text{OH})_5\cdot\text{H}_2\text{O})$ contains the AsO_4 compound. These minerals are extremely rare, even on Earth, and are unlikely to be present on Mars in sufficient quantities to be detected. Therefore, this thesis focuses on the alunite and jarosite subgroup minerals, in order to obtain results that are more directly relevant to Mars.

FTIR Spectroscopy

Infrared (IR) spectroscopy involves the study of the shifts (changes) between the vibrational energy states of atomic groups. These transitions are observed as absorption spectra, which occur when the atom absorbs energy from light. There are two main types of vibrations, stretching and bending. Stretching (ν) vibrations are observed when the bond *lengths* between the atoms change. Bending (δ) vibrations occur when the *angles* between the bonds change. In some cases, out-of-plane bending (γ) is observed, which occurs when an atom oscillates through three atoms that together form a plane. Lastly, there are symmetric and asymmetric vibrations, where either the original symmetry of the atom is maintained or it is not. These variations are shown in Figure 2.2.

Figure 2.2: Bending and Stretching in IR Spectroscopy



[http://cosid.pquim.unam.mx/McMurry/\(67\)%20Stretching%20and%20Bending%20Motions%20in%20the%20IR.jpg](http://cosid.pquim.unam.mx/McMurry/(67)%20Stretching%20and%20Bending%20Motions%20in%20the%20IR.jpg)

Review of IR Spectroscopy of Alunite and Jarosite

According to Bishop et al. (2005) (Table 2.8), there are four significant sulfate assignments: symmetric stretching at 10,194 nm for $\nu_1(\text{SO}_4)$, asymmetric stretching at 9,058 nm for $\nu_3(\text{SO}_4)$, symmetric bending at 23,202 nm for $\nu_2(\text{SO}_4)$, and asymmetric bending at 16,313 for $\nu_4(\text{SO}_4)$. The following paragraphs review the background for these assignments.

$\nu_1(\text{SO}_4)$

The first workers to observe and interpret the $\nu_1(\text{SO}_4)$ band were Serna et al. (1986) (Table 2.2), who made this assignment to the band that occurred in their spectra between 9,709 and 10,000 nm. Sasaki et al. (1998) (Table 2.3) narrowed

the assignment to refer to the band between 9,881 and 10,000 nm. Music et al. (2000) (Table 2.4) assigned $\nu_1(\text{SO}_4)$ to three different sites: one between 10,330 and 10,417 nm, one at 10,000 nm, and one at 9,259 nm. Finally, Bishop et al. (2005) had values that were clustered close to the stated proper value of 10,194 nm, but varied from 10,030 to 10,111 nm.

$\nu_2(\text{SO}_4)$

The peak energies assigned to $\nu_2(\text{SO}_4)$ have also varied to a much smaller extent relative to those for $\nu_1(\text{SO}_4)$. First Serna et al. (1986) assigned $\nu_2(\text{SO}_4)$ to a feature at 22,222 to 23,256 nm. Sasaki et al. (1998) narrowed the range from 22,222 to 22,727 nm. Music et al. (2000) assigned $\nu_2(\text{SO}_4)$ to 21,645 to 22,522 nm, and finally Bishop et al. (2005) assigned it to features occurring at 22,321 to 23,697 nm.

$\nu_3(\text{SO}_4)$

The peak energies for $\nu_3(\text{SO}_4)$ start with a range assigned by Powers et al. (1975) (Table 2.5) of 8,137 to 9,259 nm. Next, Serna et al. (1986) similarly assigned it to features at 8,163 to 9,276 nm. Sasaki et al. (1998) assigned $\nu_3(\text{SO}_4)$ to three separate sites: one at 9,259 nm, one from 9,107 to 9,191 nm, and the third at 8,197 to 8,403 nm. Music et al. (2000) also has several possible energies for $\nu_3(\text{SO}_4)$: 9,479 - 9,524 nm, 9,132 - 9,276 nm, 8,584 - 9,091 nm, and 8,368 nm.

Lastly, the most recent interpretations by Bishop et al. (2005) place $\nu_3(\text{SO}_4)$ at 9,217 - 9,233 nm, 9,091 - 9,141 nm, 8,382 - 8,584 nm, and 8,163 - 8,183 nm. The values for asymmetrical stretching vary according to most authors over a range of 1139 nm.

$\nu_4(\text{SO}_4)$

The earliest peak energies for $\nu_4(\text{SO}_4)$ were reported by Powers et al. (1975) to be 14,706 - 16,234 nm. Next, Serna et al. (1986) assigned $\nu_4(\text{SO}_4)$ to features observed at 14,599 - 15,873 nm. Then Sasaki et al. (1998) narrowed the range to 14,814 - 15,873 nm. Music et al. (2000) assigned $\nu_4(\text{SO}_4)$ to features occurring from 15,276 - 17,544 nm. Finally Bishop et al. (2005) assigned it to 14,859 - 16,077 nm. While some of these studies have values that center around the suggested 16,313 nm, the range extends for 1635 nm.

$\nu(\text{H}_2\text{O})$ and $\nu(\text{OH})$

The $\nu(\text{H}_2\text{O})$ values and the $\nu(\text{OH})$ values are all very similar. The values for $\nu(\text{OH})$ were first given by Serna et al. (1986) as 2,845 - 2,985 nm. The same range is given chronologically by Sasaki et al. (1998), then Music et al. (1998), and finally Bishop et al. (2005), who gave a single value for $\nu(\text{H}_2\text{O})$ of 2,817 nm. The only exception to this assignment is from Powers et al. (1975), who gives the

range to be from 2,856 - 2,972 nm, which fits in with the others, but also as 3,997 to 3,986 nm, which does not.

$\nu(\text{NH}_4)$

In the one study with ammonia, NH_4 , in the composition of the mineral, the values for $\nu(\text{NH}_4)$ are given by Serna et al. (1986) as 2,994 nm, 3,106 nm, 6,042 nm, and 7,003 nm.

$\delta(\text{H}_2\text{O})$ and $\delta(\text{OH})$

The in plane bending $\delta(\text{H}_2\text{O})$ was first assigned by Powers et al. (1975) to occur 13,140 - 13,477 nm, 9,970 - 9,980 nm, and 9,728 - 9,803 nm. The next assignment is given by Serna et al. (1986) as 9,940 nm, 9,728 - 9,737 nm, and 8,547 - 8,584 nm. Sasaki et al. (1998) assigns it to 9,980 nm, 9,728 - 9,794 nm. Then Music et al. (2000) assigns the in plane bending to 9,940 nm and 8,475 nm. Lastly Bishop et al. (2005) assigns it to 9,901 - 9,950 nm, 9,728 - 9,756 nm, and 9,346 - 9,425 nm. These values all are in similar ranges except for the early study of Powers which contains values higher by 400 nm

$\gamma(\text{OH})$

The out of plane bending $\gamma(\text{OH})$ has values reported by Serna et al. (1986), Sasaki et al. (1998), Music et al. (2000), and Bishop et al. (2005) that are mostly

between 16,611 and 17,857 nm. Except for one 10,989 nm value reported by Music et al. (2000), that doesn't seem to fit, they are all in that same, though rather large, range.

O-Fe or O-Al

The metal oxygen bond, in this case either being O-Fe or O-Al, is given by Power et al. (1975), Serna et al. (1986), Sasaki et al. (1998), Music et al. (2000), and Bishop et al. (2005) a very large range from 17,241 - 54,945 nm though there are no gaps in the values.

Table 2.2 IR jarosite and alunite data by Adler, H.H., and Kerr, P.F. (1965)

Jarosite 105778		Alunite 87529	
peak position (nm)	Assignment	peak position (nm)	Assignment
8439	$\nu_3(\text{SO}_4)$	8299	$\nu_3(\text{SO}_4)$
9199	$\nu_3(\text{SO}_4)$	9120	$\nu_3(\text{SO}_4)$
9940	$\nu_3(\text{SO}_4)$	9737	$\nu_3(\text{SO}_4)$
		10977	$\nu_1(\text{SO}_4)$

Table 2.3 IR jarosite and alunite data by Ross, D.S. (1974)

Jarosite, $\text{KFe}_3(\text{SO}_4)_2(\text{OH})_6$		Argentojarosite, $\text{AgFe}_3(\text{SO}_4)_2(\text{OH})_6$	
peak position (nm)	Assignment	peak position (nm)	Assignment
2915	$\nu(\text{OH})$	2759	$\nu(\text{OH})$
2981	$\nu(\text{OH})$	2789	$\nu(\text{OH})$
3067	$\nu(\text{OH})$	2976	$\nu(\text{OH})$
8403	$\nu_3(\text{SO}_4)$	8460	$\nu_3(\text{SO}_4)$
9091	$\nu_3(\text{SO}_4)$	9132	$\nu_3(\text{SO}_4)$
9728	$\nu_1(\text{SO}_4)$	9765	$\nu_1(\text{SO}_4)$
9823	$\nu_1(\text{SO}_4)$	9881	$\nu_1(\text{SO}_4)$
12658	$\delta(\text{OH})$	14815	$\nu_4(\text{SO}_4)$
14599	$\nu_4(\text{SO}_4)$	15873	$\nu_4(\text{SO}_4)$
15674	$\nu_4(\text{SO}_4)$	19685	$\delta(\text{OH})$
19531	$\delta(\text{OH})$	21053	$\nu_2(\text{SO}_4)$
20747	$\nu_2(\text{SO}_4)$	22727	$\nu_2(\text{SO}_4)$
Plumbojarosite, $\text{PbFe}_6(\text{SO}_4)_4(\text{OH})_{12}$		Alunite, $\text{KAl}_3(\text{SO}_4)_2(\text{OH})_6$	
2985	$\nu(\text{OH})$	2872	$\nu(\text{OH})$
8403	$\nu_3(\text{SO}_4)$	8547	$\nu_3(\text{SO}_4)$
9259	$\nu_3(\text{SO}_4)$	9208	$\nu_3(\text{SO}_4)$
9881	$\nu_1(\text{SO}_4)$	9709	$\nu_1(\text{SO}_4)$
10000	$\nu_1(\text{SO}_4)$	12469	$\delta(\text{OH})$
10929	$\delta(\text{OH})$	12821	$\delta(\text{OH})$
12658	$\delta(\text{OH})$	15823	$\nu_4(\text{SO}_4)$
13793	$\delta(\text{OH})$	16529	$\nu_4(\text{SO}_4)$
15576	$\nu_4(\text{SO}_4)$	19802	$\delta(\text{OH})$
15949	$\nu_4(\text{SO}_4)$	21053	$\nu_2(\text{SO}_4)$
17065	$\nu_4(\text{SO}_4)$		
20202	$\delta(\text{OH})$		
21053	$\nu_2(\text{SO}_4)$		

Table 2.4 IR jarosite data by Powers (1975)

$\text{Fe}_3(\text{CrO}_4)_2(\text{OH})_6$		$\text{KFe}_3(\text{CrO}_4)_2(\text{OD})_6$	
peak position (nm)	Assignment	peak position (nm)	Assignment
2960	v(OH)	3997	v(OH)
9980	$\delta(\text{H}_2\text{O})$	13477	$\delta(\text{H}_2\text{O})$
31153	O Fe	37175	O Fe
35336	O Fe	45249	O Fe
43478	O Fe		
50251	O Fe		
64516	O Fe		
$\text{KFe}_3(\text{SO}_4)_2(\text{OH})_6$		$\text{KFe}_3(\text{SO}_4)_2(\text{OD})_6$	
2954	v(OH)	3984	v(OH)
6116	$\delta(\text{H}_2\text{O})$	8467	$\nu_3(\text{SO}_4)$
8467	$\nu_3(\text{SO}_4)$	9259	$\nu_3(\text{SO}_4)$
9259	$\nu_3(\text{SO}_4)$	9804	$\nu_1(\text{SO}_4)$
9970	$\delta(\text{H}_2\text{O})$	13141	$\delta(\text{H}_2\text{O})$
15385	$\nu_4(\text{SO}_4)$	15337	$\nu_4(\text{SO}_4)$
15974	$\nu_4(\text{SO}_4)$	15924	$\nu_4(\text{SO}_4)$
32051	O Fe	32362	O Fe
41494	O Fe	40816	O Fe
48785	O Fe	48780	O Fe
61728	O Fe	61728	O Fe
105263	O Fe	105263	O Fe
$(\text{H}_3\text{O}^+)\text{Fe}_3(\text{SO}_4)_2(\text{OH})_6$		$\text{KAl}_3(\text{SO}_4)_2(\text{OH})_6$	
2740	v(OH)	2856	v(OH)
6127	v(H_2O)	2872	v(OH)
8403	$\nu_3(\text{SO}_4)$	8137	$\nu_3(\text{SO}_4)$
9217	$\nu_3(\text{SO}_4)$	9174	$\nu_3(\text{SO}_4)$
9980	$\delta(\text{H}_2\text{O})$	9728	$\delta(\text{H}_2\text{O})$
15384	$\nu_4(\text{SO}_4)$	14706	$\nu_4(\text{SO}_4)$
16234	$\nu_4(\text{SO}_4)$	15949	$\nu_4(\text{SO}_4)$
32680	O Fe	30120	O Al
40000	O Fe	34364	O Al
		45045	O Al
		53763	O Al
		111111	O Al
$\text{Fe}(\text{OH})\text{SO}_4$			
2892	v(OH)		
8532	$\nu_3(\text{SO}_4)$		
8787	$\nu_3(\text{SO}_4)$		
8993	$\nu_3(\text{SO}_4)$		
9452	$\nu_1(\text{SO}_4)$		

Table 2.4 cont.

peak position (nm)	Assignment	peak position (nm)	Assignment
Fe(OH)SO ₄			
9804	δ(H ₂ O)		
15385	v ₄ (SO ₄)		
15674	v ₄ (SO ₄)		
Fe(OH)(CrO ₄)		Fe(OD)CrO ₄	
2926	v(OH)	3968	O-H
9737	δ(H ₂ O)	13423	δ(H ₂ O)

Table 2.5 IR jarosite data from Serna et al. (1986)

alunite			
peak position (nm)	Assignment	peak position (nm)	Assignment
K		Na	
2849	v(OH)	2865	v(OH)
2865	v(OH)	2899	v(OH)
8163	v ₃ (SO ₄)	8163	v ₃ (SO ₄)
8583	δ(OH)	8547	δ(OH)
9217	v ₃ (SO ₄)	9091	v ₃ (SO ₄)
9709	v ₁ (SO ₄)	9709	v ₁ (SO ₄)
14599	v ₄ (SO ₄)	14925	v ₄ (SO ₄)
15873	v ₄ (SO ₄)	15873	v ₄ (SO ₄)
16611	γ(OH)	16667	γ(OH)
18939	O-Al	18692	O-Al
18939	O-Al	18692	O-Al
19608	O-Al	19231	O-Al
20325	O-Al	20619	O-Al
23256	v ₂ (SO ₄)	22727	v ₂ (SO ₄)
27397	O-Al	27778	O-Al
29851	O-Al	29586	O-Al
34247	O-Al	34247	O-Al
44248	O-Al	45045	O-Al
54054	O-Al	54945	O-Al
H ₃ O			
2865	v(OH)		
2886	v(OH)		
8163	v ₃ (SO ₄)		
8547	δ(OH)		
9132	v ₃ (SO ₄)		
9709	v ₁ (SO ₄)		
15038	v ₄ (SO ₄)		
15873	v ₄ (SO ₄)		
16667	γ(OH)		
19417	O-Al		
20408	O-Al		

Table 2.5 cont.

peak position (nm)	Assignment	peak position (nm)	Assignment
H ₃ O			
23256	v ₂ (SO ₄)		
27778	O-Al		
29412	O-Al		
34247	O-Al		
44843	O-Al		
50505	O-Al		
jarosite			
K		Na	
2950	v(OH)	2972	v(OH)
2972	v(OH)	8439	v ₃ (SO ₄)
8439	v ₃ (SO ₄)	9132	v ₃ (SO ₄)
9009	v ₃ (SO ₄)	9737	δ(OH)
9727	δ(OH)	9881	v ₁ (SO ₄)
9881	v ₁ (SO ₄)	14814	v ₄ (SO ₄)
14706	v ₄ (SO ₄)	15873	v ₄ (SO ₄)
15823	v ₄ (SO ₄)	17544	γ OH
17544	γ(OH)	19531	O-Fe
19417	O-Fe	20833	O-Fe
20747	O-Fe	22321	v ₂ (SO ₄)
22321	v ₂ (SO ₄)	28571	O-Fe
28571	O-Fe	30303	O-Fe
29851	O-Fe	38461	O-Fe
38462	O-Fe	46729	O-Fe
43478	O-Fe	48077	O-Fe
48077	O-Fe		
H ₃ O		NH ₄	
2959	v(OH)	2924	v(OH)
8333	v ₃ (SO ₄)	2994	v(NH ₄)
9174	v ₃ (SO ₄)	3105	v(NH ₄)
9881	v ₁ (SO ₄)	6042	v(NH ₄)
15873	v ₄ (SO ₄)	7003	v(NH ₄)
17544	γ(OH)	8368	v ₃ (SO ₄)
19417	O-Fe	9276	v ₃ (SO ₄)
21052	O-Fe	9940	δ(OH)
28571	O-Fe	10000	v ₁ (SO ₄)
33333	O-Fe	15267	v ₄ (SO ₄)
39216	O-Fe	15873	v ₄ (SO ₄)
43668	O-Fe	17857	γ(OH)
48780	O-Fe	19802	O-Fe
		21186	O-Fe
		22222	v ₂ (SO ₄)
		28986	O-Fe

Table 2.5 cont.

peak position (nm)	Assignment	peak position (nm)	Assignment
		NH ₄	
		31250	O-Fe
		37736	O-Fe
		49020	O-Fe

Table 2.6 IR jarosite data by Sasaki (1998)

jarosite-group			
K ⁺		NH ₄ ⁺	
peak position (nm)	Assignment	peak position (nm)	Assignment
2950	v(OH)	2924	v(OH)
2971	v(OH)	7042	v(NH ₄)
8403	v ₃ (SO ₄)	8333	V ₃ (SO ₄)
9191	v ₃ (SO ₄)	9259	V ₃ (SO ₄)
9728	δ(OH)	9980	δ(OH)
9901	v ₁ (SO ₄)	10000	V ₁ (SO ₄)
15152	v ₄ (SO ₄)	15267	V ₄ (SO ₄)
15873	v ₄ (SO ₄)	15748	V ₄ (SO ₄)
17241	γ(OH)	17241	γ(OH)
19231	O-Fe	19685	O-Fe
20921	O-Fe	21186	O-Fe
22321	v ₂ (SO ₄)	22222	V ₂ (SO ₄)
Ag ⁺		½ Pb ²⁺	
2985	v(OH)	2985	v(OH)
8403	v ₃ (SO ₄)	8368	V ₃ (SO ₄)
9158	v ₃ (SO ₄)	9009	V ₃ (SO ₄)
9794	δ(OH)	9259	V ₃ (SO ₄)
9901	v ₁ (SO ₄)	9794	δ(OH)
14925	v ₄ (SO ₄)	9843	V ₁ (SO ₄)
15873	v ₄ (SO ₄)	10000	V ₁ (SO ₄)
17637	γ(OH)	14970	V ₄ (SO ₄)
19685	O-Fe	16077	V ₄ (SO ₄)
22727	v ₂ (SO ₄)	17241	γ(OH)
		19841	O-Fe
		22727	V ₂ (SO ₄)
Na ⁺			
2971	v(OH)		
8333	v ₃ (SO ₄)		
9107	v ₃ (SO ₄)		
9737	δ(OH)		
9881	v ₁ (SO ₄)		

Table 2.6 cont.

peak position (nm)	Assignment	peak position (nm)	Assignment
Na ⁺			
14814	v ₄ (SO ₄)		
15873	v ₄ (SO ₄)		
17544	γ(OH)		
19531	O-Fe		
20833	O-Fe		
22321	v ₂ (SO ₄)		

Table 2.7 IR jarosite data by Music (2000)

(NH ₄) ₃ H(SO ₄) ₂		NH ₄ Fe ₃ (OH) ₆ (SO ₄) ₂	
peak position (nm)	Assignment	peak position (nm)	Assignment
3103	v(NH ₄)	2924	v(OH)
3286	v(NH ₄)	2994	v(NH ₄)
3502	v(NH ₄)	3106	v(NH ₄)
5770	v(NH ₄)	6042	v(NH ₄)
5952	v(NH ₄)	7003	v(NH ₄)
7072	v(NH ₄)	8368	v ₃ (SO ₄)
8475	δ(OH)	9276	v ₃ (SO ₄)
8888	v ₃ (SO ₄)	9940	δ(OH)
9259	v ₁ (SO ₄)	10000	v ₁ (SO ₄)
10417	v ₁ (SO ₄)	15267	v ₄ (SO ₄)
10989	γ(OH)	15873	v ₄ (SO ₄)
16750	v ₄ (SO ₄)	17857	γ(OH)
17544	v ₄ (SO ₄)	19802	O-Fe
22523	v ₂ (SO ₄)	21186	O-Fe
		22222	v ₂ (SO ₄)
		28986	O-Fe
		31250	O-Fe
		37736	O-Fe
		42918	O-Fe
		49020	O-Fe
Fe(OH)SO ₄		H ₃ OFe ₃ (OH) ₆ (SO ₄) ₂	
2899	v(OH)	2899	v(OH)
8584	v ₃ (SO ₄)	8621	v ₃ (SO ₄)
9091	v ₃ (SO ₄)	9132	v ₃ (SO ₄)
9479	v ₃ (SO ₄)	9524	v ₃ (SO ₄)
8889	v ₃ (SO ₄)	8850	v ₃ (SO ₄)
10331	v ₁ (SO ₄)	10000	v ₁ (SO ₄)

Table 2.7 cont.

peak position (nm)	Assignment	peak position (nm)	Assignment
Fe(OH)SO ₄		H ₃ OFe ₃ (OH) ₆ (SO ₄) ₂	
15456	v ₄ (SO ₄)	15576	v ₄ (SO ₄)
15772	v ₄ (SO ₄)	15873	v ₄ (SO ₄)
17182	v ₄ (SO ₄)	17241	v ₄ (SO ₄)
16234	v ₄ (SO ₄)	16340	v ₄ (SO ₄)
21645	v ₂ (SO ₄)	21739	v ₂ (SO ₄)

Table 2.8 IR jarosite data by Bishop (2005)

Natural jarosite 53		Natural jarosite 406	
peak position (nm)	Assignment	peak position (nm)	Assignment
2817	v(H ₂ O)	2817	v(H ₂ O)
2933	v(OH)	2937	v(OH)
2955	v(OH)	2956	v(OH)
4615	2v ₃ (SO ₄), 2δ(OH)	4604	2v ₃ (SO ₄), 2δ(OH)
4757	2v ₃ (SO ₄), 2δ(OH)	4760	2v ₃ (SO ₄), 2δ(OH)
4817	2v ₃ (SO ₄), 2δ(OH)	4817	2v ₃ (SO ₄), 2δ(OH)
4963	2v ₃ (SO ₄), 2δ(OH)	4960	2v ₃ (SO ₄), 2δ(OH)
5099	2v ₃ (SO ₄), 2δ(OH)	5099	2v ₃ (SO ₄), 2δ(OH)
6154	δ(H ₂ O)	6135	δ(H ₂ O)
8584	v ₃ (SO ₄)	8439	v ₃ (SO ₄)
9217	v ₃ (SO ₄)	9217	v ₃ (SO ₄)
9950	δ(OH)	9950	δ(OH)
10050	v ₁ (SO ₄)	10050	v ₁ (SO ₄)
15083	v ₄ (SO ₄)	15129	v ₄ (SO ₄)
15873	v ₄ (SO ₄)	15873	v ₄ (SO ₄)
19608	O-Al/ O-Fe	17241	γ(OH)
21142	O-Al/ O-Fe	19569	O-Al/ O-Fe
22371	v ₂ (SO ₄)	21053	O-Al/ O-Fe
		22422	v ₂ (SO ₄)
synthetic jarosite 440		synthetic jarosite 441	
2817	v(H ₂ O)	2817	v(H ₂ O)
2941	v(OH)	2933	v(OH)
2977	v(OH)	2954	v(OH)
4556	2v ₃ (SO ₄), 2δ(OH)	4591	2v ₃ (SO ₄), 2δ(OH)
4615	2v ₃ (SO ₄), 2δ(OH)	4750	2v ₃ (SO ₄), 2δ(OH)
4717	2v ₃ (SO ₄), 2δ(OH)	4812	2v ₃ (SO ₄), 2δ(OH)
4794	2v ₃ (SO ₄), 2δ(OH)	4941	2v ₃ (SO ₄), 2δ(OH)
4888	2v ₃ (SO ₄), 2δ(OH)	5084	2v ₃ (SO ₄), 2δ(OH)

Table 2.8 cont.

peak position (nm)	Assignment	peak position (nm)	Assignment
synthetic jarosite 440		synthetic jarosite 441	
5020	$2\nu_3(\text{SO}_4), 2\delta(\text{OH})$	6120	$\delta(\text{H}_2\text{O})$
6101	$\delta(\text{H}_2\text{O})$	8382	$\nu_3(\text{SO}_4)$
8425	$\nu_3(\text{SO}_4)$	9217	$\nu_3(\text{SO}_4)$
9140	$\nu_3(\text{SO}_4)$	9950	$\delta(\text{OH})$
9756	$\delta(\text{OH})$	10070	$\nu_1(\text{SO}_4)$
9901	$\delta(\text{OH})$	15082	$\nu_4(\text{SO}_4)$
10030	$\nu_1(\text{SO}_4)$	15873	$\nu_4(\text{SO}_4)$
14859	$\nu_4(\text{SO}_4)$	19685	O-Al/ O-Fe
15848	$\nu_4(\text{SO}_4)$	21097	O-Al/ O-Fe
17241	$\gamma(\text{OH})$	22321	$\nu_2(\text{SO}_4)$
19802	O-Al/ O-Fe		
synthetic jarosite 440		synthetic jarosite 441	
peak position (nm)	Assignment	peak position (nm)	Assignment
21008	O-Al/ O-Fe		
22471	$\nu_2(\text{SO}_4)$		
synthetic alunite 446		synthetic alunite 444	
2817	$\nu(\text{H}_2\text{O})$	2817	$\nu(\text{H}_2\text{O})$
2868	$\nu(\text{OH})$	2845	$\nu(\text{OH})$
2894	$\nu(\text{OH})$	2869	$\nu(\text{OH})$
4324	$2\nu_3(\text{SO}_4), 2\delta(\text{OH})$	4361	$2\nu_3(\text{SO}_4), 2\delta(\text{OH})$
4494	$2\nu_3(\text{SO}_4), 2\delta(\text{OH})$	4490	$2\nu_3(\text{SO}_4), 2\delta(\text{OH})$
4666	$2\nu_3(\text{SO}_4), 2\delta(\text{OH})$	4581	$2\nu_3(\text{SO}_4), 2\delta(\text{OH})$
6109	$\delta(\text{H}_2\text{O})$	4708	$2\nu_3(\text{SO}_4), 2\delta(\text{OH})$
8183	$\nu_3(\text{SO}_4)$	6109	$\delta(\text{H}_2\text{O})$
8696	$\delta(\text{H}_2\text{O})$	8164	$\nu_3(\text{SO}_4)$
9091	$\nu_3(\text{SO}_4)$	8621	$\delta(\text{H}_2\text{O})$
9425	$\nu_3(\text{SO}_4)\text{O-Al/ O-Fe}$	9234	$\nu_3(\text{SO}_4)$
9756	$\delta(\text{OH})$	9346	$\delta(\text{OH})$
10081	$\nu_1(\text{SO}_4)$	9728	$\delta(\text{OH})$
15015	$\nu_4(\text{SO}_4)$	10111	$\nu_1(\text{SO}_4)$
15924	$\nu_4(\text{SO}_4)$	14970	$\nu_4(\text{SO}_4)$
16750	$\gamma(\text{OH})$	16077	$\nu_4(\text{SO}_4)$
19531	O-Al/ O-Fe	16835	$\gamma(\text{OH})$
20491	O-Al/ O-Fe	19305	O-Al/ O-Fe
22989	$\nu_2(\text{SO}_4)$	20000	O-Al/ O-Fe
		23697	$\nu_2(\text{SO}_4)$

The Technique of Mössbauer Spectroscopy

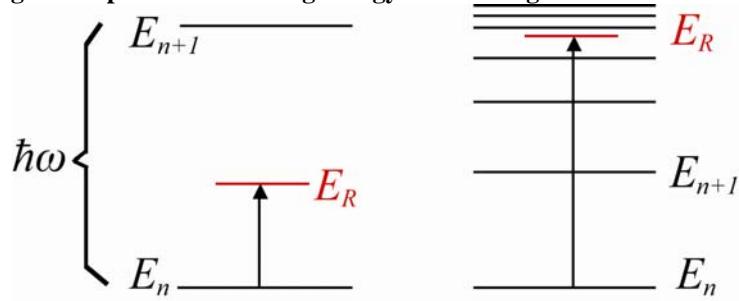
Mössbauer spectroscopy is a technique that was first discovered by Rudolf Mössbauer in 1957. It is based on an inconsistency that he noticed while doing experiments in quantum physics. In this field, theories state that electrons can obtain energy from other particles such as photons, or light particles. In an atom in equilibrium, all electrons start out at ground state, with no excess energy, orbiting the nucleus. If a particle, such as a photon, happens to pass and strike the atom, the energy from the particle will be transferred to the atom. The electron will then use this energy to try and reach an excited state or escape the atom.

An excited state is simply when the electron has more energy than it does when it is in equilibrium. While an electron that is part of a solid is in this state, it has three times the number of vibrational modes of an electron that is not in a solid state atom. A vibrational mode is easiest to explain by considering a rope with one end tied to a wall and the other held by a person. The person can move his end up or down at increasing faster speeds. At first, the rope is moved slowly and will outline one large oval, with the nodes, or immobile points, being at the ends. This is the first vibrational mode. The second occurs when two ovals are outlined by the rope, or when the center of the rope, in addition to the ends, are held still. The other vibrational modes continue to be added with faster motion,

with nodes being added for every higher vibrational state. When an electron is said to be in the first or second excited state the electron has more energy than when in equilibrium and therefore is in the first or second vibrational mode. However, an electron, unlike the example of a rope, is not in a straight line, but a circle, because it must orbit the nucleus. Therefore when a photon interacts with an atom, the electrons will change vibrational modes as described by a probability distribution. It is possible that if the photon imparts enough energy to the electron, the electron will be able to leave the atom and become its own entity.

Figure 2.3 illustrates the transfer of energy in an atom. On the left, the energy transferred to the atom was insufficient for the electron to make the jump to the next excited state. At right in the figure, the electron was given more than enough energy to pass the first excited state and it went on to the fourth. The exact energy rule, where an electron has to have the exact energy it needs to attain the next energy level, applies to all excited states, but if the electron is given enough energy it can bypass the excited states and escape the atom.

Figure 2.3: Diagram of particles receiving energy and moving to the next excited state



Mössbauer noticed the fact that a photon, if made to interact with any substance such as a liquid or a solid, will end up obtaining all of the photon's original energy. This process of energy transfer among particles is called resonant absorption. However because the atom desires equilibrium it will try to rid itself of this energy in order to return to the balanced state it was in previously. If the photon transferred to the atom a specific energy, one that is enough to allow the entire amount of energy to leave the atom, it will do so, leaving the atom with its original energy level that and allowing it to attain the equilibrium it desires.

The energy transference also can have another component. Sometimes the atom will have an initial energy of its own before the photon even hits. In this event, something else also happens: the atom, when initially struck by the photon, will recoil. This is similar to many common day occurrences, such as the recoil of a punching bag when punched. While theoretically it is possible to consider a completely still atom, meaning one with no energy of its own, it is

harder to locate one in real life, as atoms found in solids, liquids, or gases are all moving and therefore have kinetic energy.

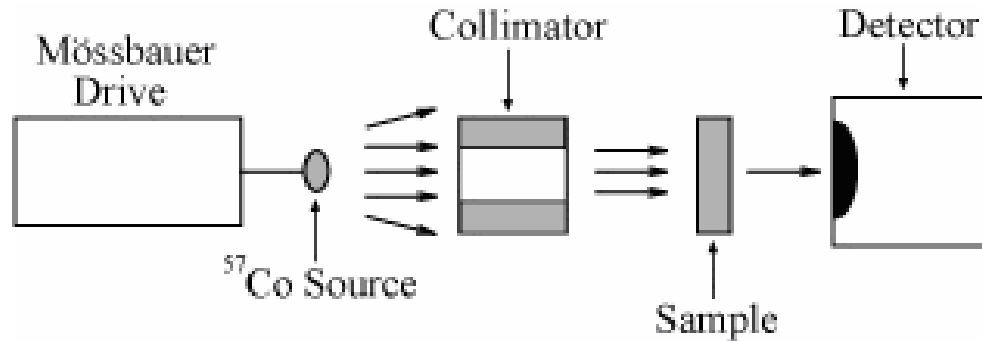
If the solid, while emitting a photon, doesn't change its vibrational mode or it only increases by one, then it is said that the solid goes through a zero- or a one- photon transition. It is possible for a zero-photon transition to occur because the entire solid will absorb the energy and cause a small amount of energy to be spread over the comparatively large mass of the solid, making the amount of energy negligible. In Mössbauer spectroscopy, the percentage of the time that this happens is called the recoil-free fraction, meaning the number of times that the atom doesn't recoil on impact. The fraction can be determined by a formula, which shows that the value of the recoil-free fraction is dependent on temperature, where larger temperatures lead to larger vibrational amplitudes. The Mössbauer effect cannot take place in liquids or gases because the recoil-free fraction will always end up being zero.

Energy interactions had already been studied. While Mössbauer was doing his research, he obtained data that was contrary to the expectations of the previous theories. When the temperature was decreased, it was expected that the absorption of the energy by the atom would become smaller. This was predicted by the fact that the kinetic energy of the atom is reliant on the

temperature. Therefore if the temperature becomes lower, the atom would have less energy, and it wouldn't recoil to the extent that it would at room temperature. That is what was theoretically predicted, but in the actual studies, the absorption decreased as the temperature lowered. This result gave rise to further studies by Mössbauer and to the discovery of the Mössbauer effect, which is the zero-photon transition.

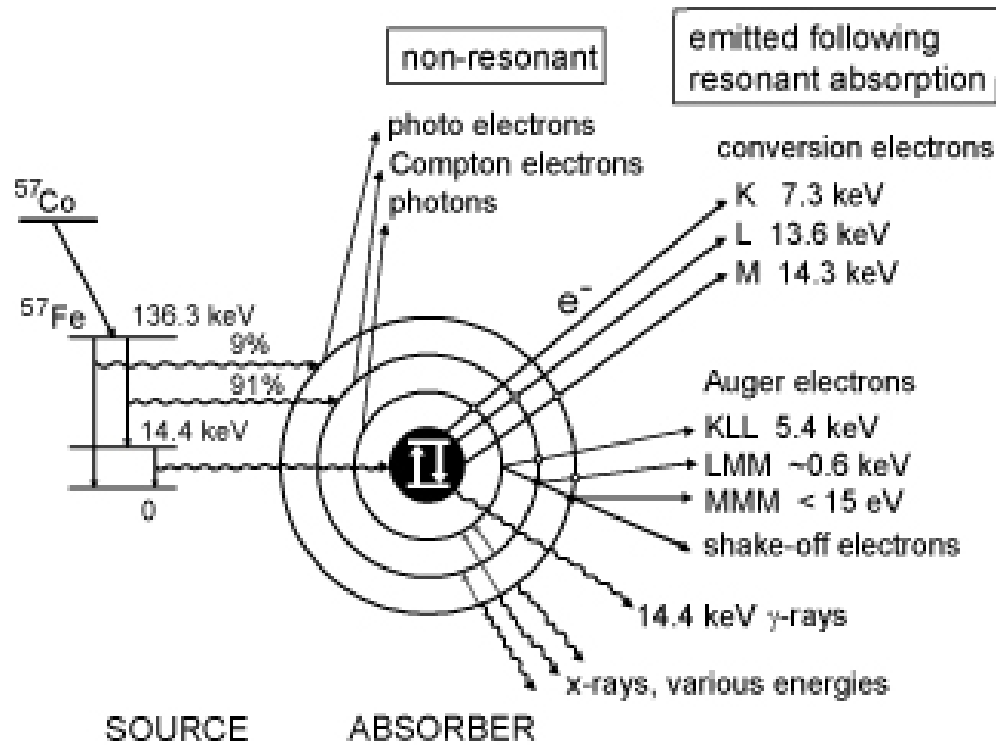
Mössbauer spectroscopy, invented by Mössbauer in 1957, measures the resonant absorption in solids using gamma-rays, which take the place of photons in the examples discussed above. The setup of the spectrometer consists of an oscillator that moves the radioactive source back and forth relative to the sample, giving it a velocity, which in turn gives a higher energy to the gamma-rays. Because of this, the velocity measurement, millimeters per second (mm/s), is also used as the energy unit. The spectrum is really measuring the difference between the velocity at which the photon was emitted and the percentage at which it was absorbed by the sample. The gamma rays travel through the sample and into the detector, which records the ending energy levels of the particles. This process is seen in the Figure 2.4.

Figure 2.4: Illustration of Mössbauer process



Iron is the element measured in Mössbauer spectroscopy because of the length of its lifetime. It neither decays too slowly nor too quickly, it is able to be used with many other naturally occurring isotopes, and it has a small energy that results from nuclear transitions and therefore its recoil-free fraction is large. A typical Mössbauer source is ^{57}Co , which is the parent isotope to ^{57}Fe , meaning that ^{57}Co decays into ^{57}Fe . Most of the time, the decay of the cobalt ends with an energy of 14.4eV. Many events can happen at this energy level, such as the emission of a gamma-ray or the emission of an electron. These possibilities are displayed in Figure 2.5, where the radioactive source, seen on the left, is shown emitting gamma-rays at different possible energy levels. The gamma-rays are then shown interacting with the atom and all the possible outcomes with their ending energy level are shown.

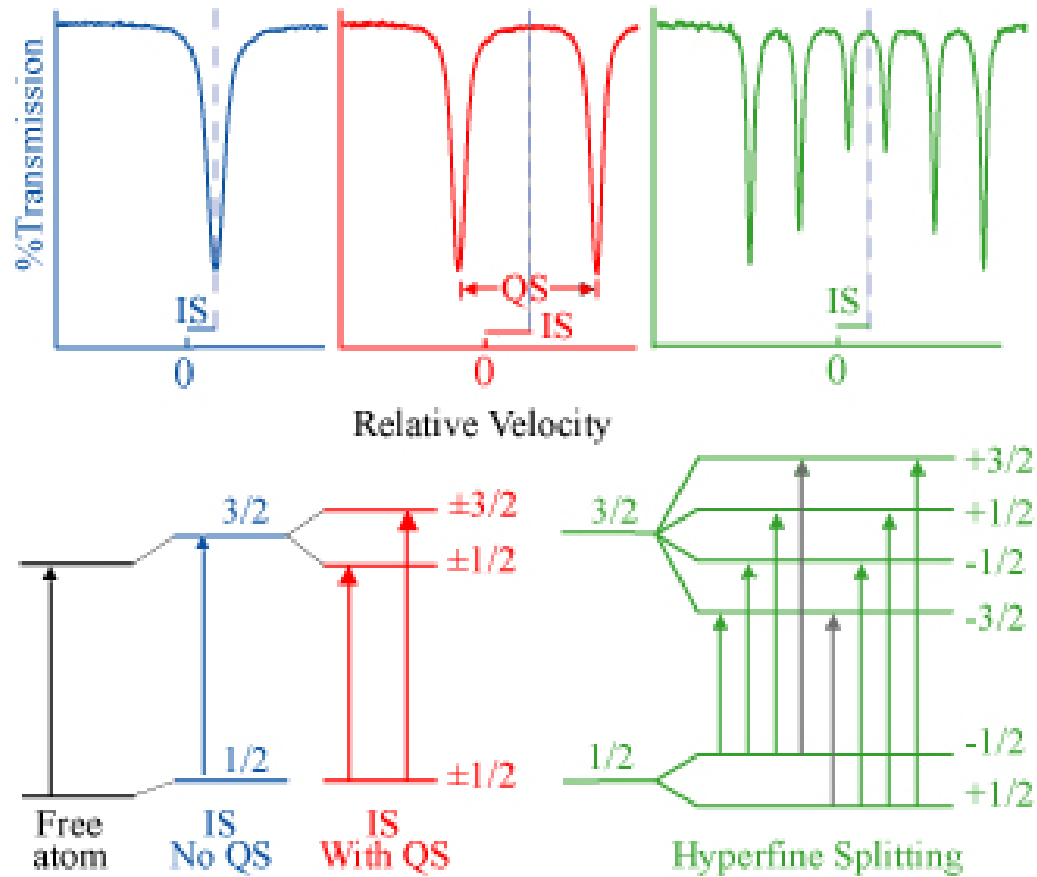
Figure 2.5: Diagram of the various paths an electron



A Mössbauer spectrum consists of a set of peaks, either a doublet (a line with two peaks) or a sextet (a line with six peaks) that describes a specific state of the iron nucleus. This is what makes the Mössbauer a useful tool. The energy levels of an atom can also be changed, shifted or split apart, by the electronic environment in what called is hyperfine interaction. Because the environment and the absorbing material do not have the same electric energy, the absorption spectra will have a non-zero relative energy. This is shown by having a non-zero velocity show up in the transmission spectrum; a parameter called the isomer shift (δ) (See Figure 2.6, left hand side). This shift is a result of the nuclear and the surrounding electronic environment having different charge distributions.

As discussed above, there is a difference of charge between the electronic environment and the atom. This causes an electronic field to arise in the solid and causes the energy levels in the atom to split. This is the second parameter called quadrupole splitting (Δ), which causes the doublets or sextets in the spectrum to have multiple peaks (See Figure 2.6, middle). Iron contains a magnetic moment so its energy levels can be changed if there is an external magnetic field or if the mineral is magnetically ordered. This will cause a magnetic hyperfine (Zeeman) splitting, which causes the atom's energy levels to split into six and creates a sextet. These three parameters, the isomer shift, quadrupole splitting, and magnetic hyperfine interactions, can be used to identify what state the iron atom is in. Iron atom locations are different for different groups of minerals and it is therefore possible to use the values obtained from the parameters of the spectra to narrow down the possibilities in order to identify an unknown mineral.

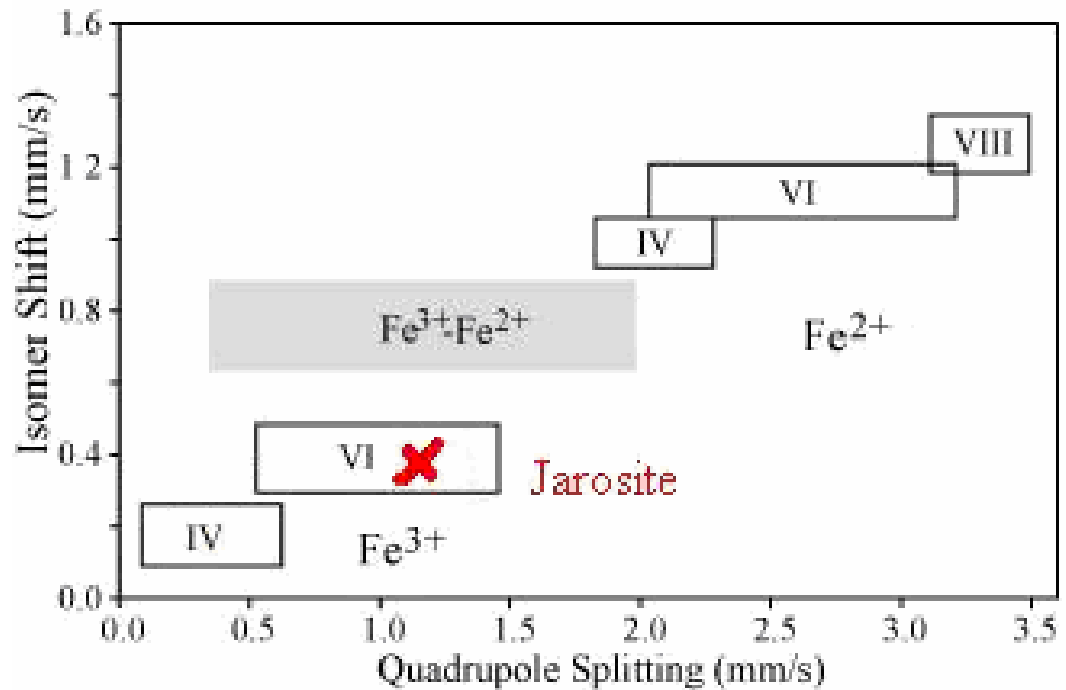
Figure 2.6: Diagram of the parameters of Mössbauer



The iron atom can only exist in a few states, so many minerals have Mössbauer parameters that are very similar to others. Below is a figure that shows where the different groups of iron generally fall in terms of isomer shift versus quadrupole splitting. It is easy to see that the ferric, Fe^{3+} , iron which is missing three electrons, has an isomer shift between 0.1 - 0.5 mm/s and a quadrupole splitting between 0.3 - 1.3 mm/s. Ferrous, Fe^{2+} , iron that is missing two electrons, has an isomer shift over 1.0 mm/s and a quadrupole splitting above 1.5 mm/s. In spectra it is very easy to tell ferric iron from ferrous iron because of

the obvious distinctions in their locations on this graph. In Figure 2.7, the red x marks where jarosite usually falls on the continuum.

Figure 2.7: Isomer shift vs. quadrupole splitting



MÖSSBAUER STUDIES OF JAROSITE AND ALUNITE

The isomer shift and quadrupole splitting ascribed to Fe³⁺ in octahedral coordination in jarosite have stayed fairly consistent in the literature (Table 2.6). The average isomer shifts lies in the area of 0.30 mm/s to 0.45 mm/s, with a slight concentration around the upper end of 0.30 mm/s (Table 2.9). The lower exceptions are 0.20 mm/s (Waanders et al., 2003) and 0.29 mm/s (Fajardo et al., 1999). Isomer shift values that are over 0.45 mm/s are more plentiful, including

0.54 mm/s (Herzenberg, 1966), 0.48 mm/s for a natrojarosite (Grinkevich et al., 1963), 0.46 mm/s also found in a coal (Tanejas et al., 1984), of 0.61 mm/s and 0.63 mm/s (van der Kraan et al., 1984), a jarosite with an isomer shift of 0.47 mm/s and a burning star jarosite with an isomer shift of 0.48 mm/s (Audley et al., 1986), 0.50 mm/s (Pax et al., 1988). These exceptions could indicate that jarosite is not really present, or it could be that some of the sample preparation processes altered the mineral in a way that affected the iron sites.

A few studies have recorded jarosite Mössbauer spectra at low temperatures. Huggins et al. (1983) reported values of 0.44 - 0.52 mm/s at 77K. In the next study, Tanejas et al. (1984) recorded values of 0.39- 0.42 mm/s at a temperature of 77K. Gancedo et al. (1992) reported values of 0.4- 0.50 mm/s at 17K. Next, Herbert et al. (1997) reported values of 0.48- 0.51 mm/s at 77K. Ahmed et al. (1999) recorded values of 0.43- 0.47 mm/s at 80K. Then Verma et al. (2000) reported values of 0.37 mm/s at 25K and 0.39 mm/s at 225K. Next Ribeiro et al. (2003) recorded values of 0.45 and 0.44 mm/s at 80K. Most recently, Rodriguez et al. (2005) reported values of 0.47mm/s at 77K, 0.51 mm/s at 20K, 0.50 mm/s at 4.2K, and 0.49 mm/s at 2K.

There are only two studies that have reported isomer shift values for spectra at higher than room temperatures. Those values are 0.43 mm/s at 470K-

480K (Seymour, 1993) and 0.37 mm/s at 425K (Verma et al., 2000). Those values fall in the range observed for all the room temperature values.

The quadrupole splitting stays between the broad range of 1.00 mm/s and 1.22 mm/s. More values occur between 1.13 mm/s and 1.18 mm/s (see Table 2.9).

The major deviations from this range are 0.54 mm/s for the standard formula of jarosite (Herzenberg et al., 1966), are mercury enriched jarosite at 0.91 mm/s (Leclerc, 1980), 0.85 mm/s and 0.96 mm/s for coal jarosite (Tanejas et al., 1984), burning star jarosite at 0.95 mm/s (Audley et al., 1986), three values between 0.982 mm/s and 0.997 mm/s for hydronium jarosite (Music et al., 1994), 1.86 mm/s (Herbert, 1997), one negative value of -0.13 mm/s accompanied by, 0.36 mm/s, 0.61 mm/s, 0.86 mm/s, 1.44 mm/s and 1.49 mm/s for ammoniojarosite (Ristic et al., 2000), jarosite at 0.96 mm/s (Waanders et al., 2003), and 1.32 mm/s (Ribeiro et al., 2003).

For the studies containing lower temperature spectra of jarosite, the average quadrupole splitting seems to be the same, somewhere between 1.00 mm/s and 1.22 mm/s (Tanejas et al., 1984, Gancedo et al., 1992, Herbert, 1997, Ahmed et al., 1999, Verma et al., 2000, Klingelhofer et al., 2004, Rodriguez et al., 2005). The exceptions are a coal-containing jarosite with a value of 0.93 mm/s at 77K

(Tanejas et al., 1984), 1.27 mm/s and 1.29 mm/s run at 17K (Gancedo et al., 1992), a value of 1.39 mm/s run at 77K (Herbert, 1997), 1.24 mm/s run at 225K (Verma et al., 2000), 1.26 mm/s and 1.25 mm/s run at 80K (Ribeiro et al., 2003), and the impossible values of -0.15 mm/s, -0.16 mm/s , and -0.14 mm/s run at 20K, 4.2K, and 2K (Rodriguez et al., 2005).

Table 2.9 Mössbauer parameters of jarosite

Formula	IS (mm/s)	QS (mm/s)	Temp (K)
Grinkevich, A.Z. et al. (1963)			
NaFe ₃ (SO ₄) ₂ (OH) ₆	0.48	1.00	RT
KFe ₃ (SO ₄) ₂	0.45	1.10	RT
Hryniewicz, A.Z. et al. (1965)			
H ₃ OFe ₃ (SO ₄) ₂ (OH) ₆	0.05	1.00	RT
NaFe ₃ (SO ₄) ₂ (OH) ₆	0.05	1.05	RT
KFe ₃ (SO ₄) ₂ (OH) ₆	0.05	1.15	RT
NH ₄ Fe ₃ (SO ₄) ₂ (OH) ₆	0.05	1.15	RT
Pb[Fe ₃ (SO ₄) ₂ (OH) ₆] ₂	0.05	1.15	RT
KFe _{2.5} Al _{0.5} (SO ₄) ₂ (OH) ₆	0.05	1.25	RT
Herzenberg, C.L., et al. (1966)			
KFe ₃ (OH) ₆ (SO ₄) ₂	0.30	0.54	RT
Takano, M. et al. (1968)			
NH ₄ Fe ₃ (SO ₄) ₂ (OH) ₆	0.43	1.22	RT
NaFe ₃ (SO ₄) ₂ (OH) ₆	0.43	1.20	RT
KFe ₃ (SO ₄) ₂ (OH) ₆	0.43	1.24	RT
Afanasev, A.M., et al. (1974)			
H ₃ OFe ₃ (SO ₄) ₂ (OH) ₆	0.59	1.14	16.3
H ₃ OFe ₃ (SO ₄) ₂ (OH) ₆	0.60	1.16	17.4
H ₃ OFe ₃ (SO ₄) ₂ (OH) ₆	0.59	1.13	20.1
H ₃ OFe ₃ (SO ₄) ₂ (OH) ₆	0.59	1.13	24.7
H ₃ OFe ₃ (SO ₄) ₂ (OH) ₆	0.59	1.13	77
Pb[Fe ₃ (SO ₄) ₂ (OH) ₆] ₂	0.63	1.20	44.8
Pb[Fe ₃ (SO ₄) ₂ (OH) ₆] ₂	0.60	1.22	51.3
Pb[Fe ₃ (SO ₄) ₂ (OH) ₆] ₂	0.52	1.17	77
KFe _{2.5} Al _{0.5} (SO ₄) ₂ (OH) ₆	0.58	1.20	4.2
KFe _{2.5} Al _{0.5} (SO ₄) ₂ (OH) ₆	0.58	1.25	5.2
KFe _{2.5} Al _{0.5} (SO ₄) ₂ (OH) ₆	0.66	1.27	25.2
KFe _{2.5} Al _{0.5} (SO ₄) ₂ (OH) ₆	0.58	1.27	33.3
KFe _{2.5} Al _{0.5} (SO ₄) ₂ (OH) ₆	0.66	1.28	39.5
KFe _{2.5} Al _{0.5} (SO ₄) ₂ (OH) ₆	0.58	1.29	45.7
KFe _{2.5} Al _{0.5} (SO ₄) ₂ (OH) ₆	0.59	1.27	48.6
KFe _{2.5} Al _{0.5} (SO ₄) ₂ (OH) ₆	0.58	1.27	55.5
KFe _{2.5} Al _{0.5} (SO ₄) ₂ (OH) ₆	0.56	1.24	77
Johnston (1977)			
K _{0.56} Na _{0.39} H ₃ O _{0.05} (Al _{1.16} Fe _{0.84}) ₃ (SO ₄) ₂ (OH) ₆	0.16	1.24	RT
Huffman, G.P., et al. (1978)			
(Na,K)Fe ₃ (SO ₄) ₂ (OH) ₆	0.368	1.207	RT
Leclerc, A. (1980)			
H ₃ O ⁺	0.39	1.01	RT
Na ⁺ (1)	0.38	1.06	RT
Na ⁺ (2)	0.38	1.07	RT

Table 2.9 cont.

Formula	IS (mm/s)	QS (mm/s)	Temp (K)
Leclerc, A. (1980)			
K ⁺	0.38	1.13	RT
Rb ⁺	0.39	1.13	RT
Ag ⁺	0.39	1.01	RT
NH ⁴⁺	0.39	1.12	RT
Tl ⁺	0.39	1.08	RT
PB ²⁺ (1)	0.39	1.17	RT
PB ²⁺ (2)	0.39	1.12	RT
PB ²⁺ (3)	0.38	1.22	RT
Hg ²⁺	0.39	0.91	RT
Huggins, F.E. et al. (1983)			
jarosite (coal A highwall)	0.44	1.14	77K
jarosite (coal a middle)	0.52	1.10	77K
jarosite (coal b unoxidized)	0.44	1.10	77K
jarosite (coal b highwall)	0.46	1.15	77K
jarosite (coal b middle)	0.51	1.10	77K
jarosite (coal b outcrop)	0.48	1.10	77K
Tanejas, S.P., et al. (1984)			
jarosite (coal4)	0.41	1.05	RT
jarosite (coal5)	0.46	1.00	RT
Tanejas, S.P., et al. (1984)			
jarosite(coal 1)	0.42	1.06	RT
jarosite(coal 1)	0.41	0.93	77K
jarosite (coal 2)	0.42	0.85	RT
jarosite (coal 3)	0.44	0.96	RT
jarosite (coal 4)	0.45	1.05	RT
jarosite (coal 4)	0.42	1.08	77K
jarosite (coal 5)	0.37	1.01	RT
jarosite (coal 5)	0.39	1.05	77K
jarosite (coal 7)	0.41	1.05	RT
jarosite (coal 7)	0.42	1.08	77K
jarosite (coal 8)	0.46	1.00	RT
Van der Kraan, A.M., et al. (1984)			
jarosite	0.63	1.14	RT
jarosite	0.61	1.15	RT
Audley, G.J., et al. (1986)			
jarosite (hartshorneMV)	0.47	1.02	RT
jarosite(hartshorne HVA)	0.38	1.08	RT
jarosite(herrin high sulphur)	0.34	1.19	RT
jarosite(burning star)	0.48	0.95	RT
jarosite(harrisburgh)	0.36	1.02	RT
jarosite(wyodak)	0.39	1.24	RT

Table 2.9 cont.

Formula	IS (mm/s)	QS (mm/s)	Temp (K)
Pax, R.A. et al. (1988)			
jarosite	0.43	1.10	RT
jarosite	0.50	1.00	RT
Komaraus, J.L. et al. (1988)			
jarosite (WK 10c)	0.37	1.12	RT
Gracia, M. et al. (1990)			
jarosite (pontes coal)	0.41	1.08	RT
jarosite (pontes coal 4h/383K)	0.39	1.14	RT
jarosite (pontes coal 50h/383K)	0.38	1.05	RT
jarosite (pontes coal 4h/423K)	0.37	1.02	RT
jarosite (pontes coal 20h/423K)	0.34	1.04	RT
jarosite (pontes coal 4h/463K)	0.33	1.16	RT
jarosite (mierama coal)	0.37	1.10	RT
jarosite (mierama coal 4h/383K)	0.38	1.12	RT
jarosite (mierama coal 50h/383K)	0.39	1.15	RT
jarosite (mierama coal 20h/423K)	0.35	1.15	RT
jarosite (mierama coal 20h/423K)	0.35	1.15	RT
jarosite (mierama coal 20h/423K)	0.35	1.15	RT
jarosite (mierama coal 4h/463K)	0.38	1.12	RT
jarosite (pontes coal 2h/150W/423K)	0.37	1.18	RT
jarosite (pontes coal 24h/15W/423K)	0.36	1.17	RT
jarosite (pontes coal 8h/250W/423K)	0.35	1.15	RT
jarosite (meirama coal 32h/150W/423K)	0.36	1.08	RT
Gancedo, J.R. et al. (1992)			
jarosite ("C-py" 0)	0.34	1.12	RT
jarosite ("C-py" 0)	0.4	1.27	17K
jarosite ("C-py" I)	0.3	1.1	RT
jarosite ("C-Or" 0)	0.35	1.12	RT
jarosite ("C-Or" I)	0.35	1.13	RT
jarosite ("C-Or" I)	0.5	1.1	17K
jarosite ("C-Or" II)	0.35	1.1	RT
jarosite ("C-Or" II)	0.42	1.29	17K
Seymour, K. et al. (1993)			
$H_3OFe_3(SO_4)_2(OH)_6$	0.40	1.00	RT
$NaFe_3(SO_4)_2(OH)_6$	0.40	1.05	RT
$KFe_3(SO_4)_2(OH)_6$	0.40	1.15	RT
$NH_4Fe_3(SO_4)_2(OH)_6$	0.40	1.15	RT
$Pb[Fe_3(SO_4)_2(OH)_6]_2$	0.40	1.15	RT
$NH_4Fe_3(SO_4)_2(OH)_6$	0.43	1.22	480K
$NaFe_3(SO_4)_2(OH)_6$	0.43	1.20	470K

Table 2.9 cont.

Formula	IS (mm/s)	QS (mm/s)	Temp (K)
Seymour, K. et al. (1993)			
$\text{KFe}_3(\text{SO}_4)_2(\text{OH})_6$	0.43	1.22	470K
Music, S. et al. (1994)			
$\text{H}_3\text{OFe}_3(\text{SO}_4)_2(\text{OH})_6$	0.38	1.00	RT
$\text{H}_3\text{OFe}_3(\text{SO}_4)_2(\text{OH})_6$	0.36	1.00	RT
$\text{H}_3\text{OFe}_3(\text{SO}_4)_2(\text{OH})_6$	0.38	1.13	RT
$\text{H}_3\text{OFe}_3(\text{SO}_4)_2(\text{OH})_6$	0.38	1.01	RT
$\text{H}_3\text{OFe}_3(\text{SO}_4)_2(\text{OH})_6$	0.38	1.00	RT
Morris, R.V., et al. (1996)			
jarosite(natro)	0.36	1.19	RT
jarosite, smectice, quartz, kaolinite	0.33	1.2	RT
gypsum, smectice, mica, jarosite	0.33	1.22	RT
quartz, gypsum, jarosite	0.33	1.2	RT
<1mm:jarosite, plagioclase	0.38	1.19	RT
<5 μm : jarosite	0.36	1.15	RT
Herbert, R.B., Jr. (1997)			
jarosite (J14)	0.39	1.1	RT
jarosite (J14)	0.49	1.16	77K
jarosite (1092)	0.38	1.12	RT
jarosite (1092)	0.49	1.22	77K
jarosite (1093)	0.39	1.01	RT
jarosite (1093)	0.51	1.11	77K
jarosite (1093)	0.36	1.86	RT
jarosite (1093)	0.48	1.39	77K
Ahmed, M.A. et al. (1999)			
$(\text{Na,K})\text{Fe}_2(\text{SO}_4)_3 \cdot n\text{H}_2$	0.36	1.22	RT
$(\text{Na,K})\text{Fe}_2(\text{SO}_4)_3 \cdot n\text{H}_2$	0.44	1.15	80K
$(\text{Na,K})\text{Fe}_2(\text{SO}_4)_3 \cdot n\text{H}_2$	0.36	1.17	RT
$(\text{Na,K})\text{Fe}_2(\text{SO}_4)_3 \cdot n\text{H}_2$	0.47	1.2	80K
$(\text{Na,K})\text{Fe}_2(\text{SO}_4)_3 \cdot n\text{H}_2$	0.37	1.12	RT
$(\text{Na,K})\text{Fe}_2(\text{SO}_4)_3 \cdot n\text{H}_2$	0.43	1.2	80K
$(\text{Na,K})\text{Fe}_2(\text{SO}_4)_3 \cdot n\text{H}_2$	0.37	1.09	RT
$(\text{Na,K})\text{Fe}_2(\text{SO}_4)_3 \cdot n\text{H}_2$	0.47	1.15	80K
Fajardo, M. et al. (1999)			
jarosite (Fer)	0.4	1	RT
jarosite (Fer1.4s)	0.31	1	RT
jarosite (Fer1.6s)	0.29	1	RT
jarosite (Hon)	0.4	1	RT
jarosite (Hon1.4s)	0.4	1	RT
jarosite(Hon1.6s)	0.4	1	RT

Table 2.9 cont.

Formula	IS (mm/s)	QS (mm/s)	Temp (K)
Fajardo, M. et al. (1999)			
jarosite (Uri)	0.4	1	RT
jarosite (Uri1.4s)	0.36	1	RT
jarosite (Uri1.6s)	0.36	1	RT
Ristic, M. et al. (2000)			
NH ₄ Fe ₃ (OH) ₆ (SO ₄) ₂	0.4	0.86	RT
NH ₄ Fe ₃ (OH) ₆ (SO ₄) ₂	0.42	1.44	RT
NH ₄ Fe ₃ (OH) ₆ (SO ₄) ₂	0.65	0.36	RT
NH ₄ Fe ₃ (OH) ₆ (SO ₄) ₂	0.3	0.61	RT
NH ₄ Fe ₃ (OH) ₆ (SO ₄) ₂	0.4	1.49	RT
NH ₄ Fe ₃ (OH) ₆ (SO ₄) ₂	0.49	-0.13	RT
Verma, H.C. et al. (2000)			
jarosite	0.37	1.12	RT
jarosite	0.37	1.12	RT
jarosite	0.37	1.19	RT
jarosite (HCl treated)	0.36	1.09	RT
jarosite (HNO ₃ treated)	0.35	1.12	RT
jarosite	0.36	1.1	RT
jarosite	0.37	1.15	RT
jarosite	0.37	1.05	RT
jarosite	0.4	1.17	RT
jarosite	0.37	1.14	25K
jarosite	0.39	1.24	225K
jarosite	0.36	1.12	325K
jarosite	0.38	1.07	365K
jarosite	0.37	1.1	425K
Ahmed, M.A. et al. (2003)			
(Na,K)Fe ₂ (SO ₄) ₃ .nH ₂	0.37	1.1	RT
Waanders, F.B., et al. (2003)			
jarosite (5)	0.2	0.96	RT
Reyes, F., et al. (2003)			
jarosite (V4N1)	0.36	1.14	RT
jarosite (V GASOSA)	0.36	1.08	RT
Lal, R., and Sharma, N.D. (2003)			
jarosite	0.36	1.12	RT
Ribeiro, F.R., et al. (2003)			
jarosite	0.36	1.32	RT
jarosite	0.45	1.26	80K
jarosite (NaOH treated)	0.33	1.11	RT
jarosite (NaOH treated)	0.44	1.25	80K

Table 2.9 cont.

Formula	IS (mm/s)	QS (mm/s)	Temp (K)
Klingelhofer, G., et al. (2004)			
jarosite(average outcrop matrix)	0.39	1.22	200-280K
jarosite(berrybowl)	0.39	1.22	200-280K
Eneroth, E. et al. (2004)			
jarosite	0.38	1.06	RT
Rodriguez, N., et al. (2005)			
jarosite	0.38	1.19	RT
jarosite	0.47	1.18	77K
jarosite	0.51	-0.15	20K
jarosite	0.5	-0.16	4.2K
jarosite	0.49	-0.13	2K

METHODS

Synthesis of the samples used in this thesis was done by G. Brophy at Amherst College in the early 1960's. Brophy (1965) created a series of synthetic alunite and jarosites with varying aluminum and iron contents. From this larger suite of samples, we obtained a group that corresponds to jarosite (Fe^{3+} -rich) compositions. The method used by Brophy is described by Fairchild (1933). The samples were made from a 1 to 3 molar ratio of potassium sulphate to ferric sulphate with an extra 20 percent of ferric sulphate. This mixture was then dissolved in sulphuric acid and heated. The end product depended on the temperature that was used to heat the reactants. The mixture was heated for 24 hours at 110°C and then at 180°C for another 24 hours, so that jarosite was produced.

Variations on this process have produced similar results. Parker (1954) produced alunite by dissolving potassium sulphate with $\text{Al}(\text{SO}_4)_3 \cdot 18\text{H}_2\text{O}$ in water. Then for 2 to 4 days, the solution was refluxed at its boiling point. Alunite was produced but there was excess water in the mineral. Barrington (1957) used the same method as Parker (1954), but used sulphuric acid as the solvent and higher concentrations of starting reactants.

The jarosites used in this study, as described in Brophy (1965), were made using the Fairchild method. He dissolved the alkali sulfate and $\text{Fe}_2(\text{SO}_4)_3$ in sulphuric acid and placed the product in an oil bath heated to 114°C for 72 hours. The product was then removed from heat, washed, and air dried.

The end product was analyzed by Brophy (1965) in several different ways. The water content was tested by weighing the jarosite and then heating it and weighing it again. The iron was tested by titration using ceric ion. The sulphate quantity was measured by separating BaSO_4 as a solid from the rest of the material. The sodium and potassium content was measured by flame photometer. All the samples were heated to 500°C before testing. X-ray diffraction, both film and diffractometer, were done on the powdered samples and showed that the materials were indeed jarosite. The varying compositions of the samples, based on Brophy (1965), are shown in Table 3.1. There were two sets of samples, 1 – 18 excluding number 4 that had been heated to 300°C and were labeled with a b, the second was a set of samples that included numbers 1 – 8 also excluding 4 that had been heated to 248°C .

In the year 2000, Janice Bishop contacted Darby Dyar to inquire if the Brophy samples were available for further study. Gerry Brophy made a special visit back to campus, and other faculty in the Department of Geology at Amherst

College, and looked high and low for the suite of samples. Unfortunately the samples could not be located. In May of 2005, the Department was preparing to move to a new building. In the process of packing, Peter Crowley spotted two drawers containing test tubes and crucibles of yellow material. He remembered the early inquiry and made arrangements for the samples to come to Mount Holyoke College. Comparisons between the samples described in Brophy (1965) and the contents of the drawers quickly made it apparent that the missing suite of samples had been discovered.

Table 3.2: Jarosite $\text{H}_3\text{ONaKFe}_3(\text{SO}_4)_2(\text{OH})_6$ Compositions from Brophy (1965)

	H ₃ O	K	Na
syn1	10	86	4
syn2	24	74	2
syn3	25	74	1
syn5	29	70	1
syn6	32	67	1
syn7	34	60	7
syn8	33	57	10
syn9	42	56	2
syn10	42	55	3
syn11	35	49	16
syn12	51	47	2
syn13	28	4	68
syn14	19	3	78
syn15	27	2	72
syn16	34	1	65
syn17	16	1	83
syn18	17	0	83

Infrared Methods

Near-infrared (NIR) reflectance spectra were measured at the Reflectance Experiment Laboratory (RELAB) at Brown University using a reflectance spectrometer. The samples were purged of water overnight and were then calibrated with a rough gold surface in a moisture-free environment. The spectra were collected from 900 – 4760 nm. The interferometer's mirror moved at a velocity was 0.4747 cm/sec. The light passed through an aperture with the size of 25, which gives a diameter of 25 mm. Exactly 200 scans were performed of each sample at a resolution of 5000 nm.

Mid-infrared (Mid-IR) spectra were also collected at RELAB, again purging the samples overnight and using a rough gold surface as a foil. The range covered the mid-IR region starting at 1600 and ending at 28500 nm. The velocity of the interferometer's mirror was 0.3165 cm/sec. The same aperture was used. Exactly 100 scans were taken of each sample with a resolution of 5000 nm each.

Mössbauer Methods

Mössbauer mounts were created by mixing 30 mg of ground synthetic jarosites with ground sugar in order to fill up the volume of the sample mount, which is a plastic washer. The powder is held in place in the washer by kapton tape on one side and a nylon flat disk on the other. The samples were then run on the Mössbauer spectrometer in the Mineral Spectroscopy Lab at Mount Holyoke for 6 hours each. One jarosite sample with the composition of $\text{H}_3\text{O}_{.24}\text{Na}_{.02}\text{K}_{.74}\text{Fe}_3(\text{SO}_4)_2(\text{OH})_6$ was chosen as a representative sample of the jarosite suite. It was run at temperatures from 16 to 75K in 5K increments, then 90 to 270K in 25K increments, all at low He gas pressure. Because the sample was high in iron and the Mössbauer source was new (100 mCi), each spectrum was acquired for only one hour, which still resulted in non-resonant (baseline) counts for each spectrum.

The Mössbauer spectrometer was a WEB Research Co. model W100 unit, equipped with a Janus closed-cycle He refrigerator. Results were calibrated against α -Fe foil. Spectra were fit with quadrupole splitting distributions (QSD) and hyperfine field distributions using the method of (Wivel and Mørup, 1981). An average correlation between the isomer shift and quadrupole splitting of Fe^{2+} was assumed, in all fits to the data.

The jarosite spectra were fit with either three or four doublets and one or no sextet, depending on the specific jarosite, as all the spectra are slightly different. Table 3.2 shows various fits to sample 6B, though a similar process was undertaken for each spectrum. The table shows the evolution of χ^2 the number of doublets and sextets is increased, starting with one, then two and three ferric doublets; finally, the fourth fit has the addition of a sextet.

Table 3.2 Jarosite 6B fit with an assortment of different parameters

Jarosite 6B				
MF				586.5
Γ				0.25
δ				0.77
Δ				0.92
Area				2.1
Γ	0.32	0.23	0.26	0.25
δ	0.39	0.39	0.39	0.39
Δ	1.21	1.24	1.25	1.27
Area	100.0	39.4	45.1	44.4
Γ		0.38	0.25	0.25
δ		0.39	0.38	0.38
Δ		1.01	1.06	1.06
Area		60.6	28.0	25.1
Γ			0.40	0.41
δ			0.40	0.40
Δ			0.81	0.84
Area			26.9	28.4
χ^2	67	14	7	6

The value of χ^2 demonstrates the fact that the fit improves steadily with the addition of new components. Generally, values of χ^2 that are less than 10 are considered optimal. Thus, the χ^2 seems to indicate that fits with three doublets with or without the sextet are probably acceptable, because the sextet has very

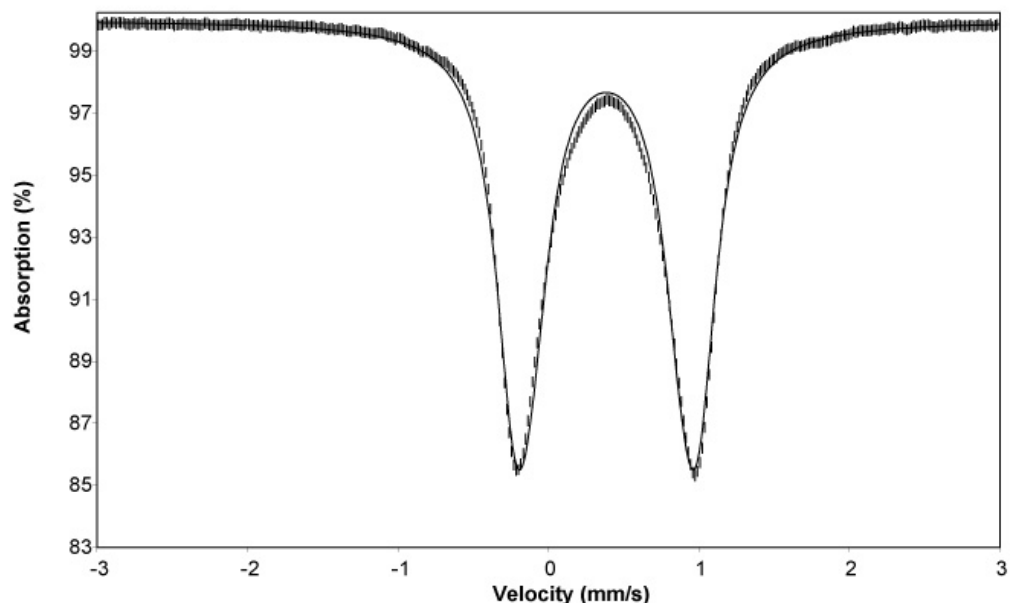
little area at room temperature. Even though its area is only 2%, it is still important for the sextet to be included, because it is seen in almost all of the other jarosite samples and it does improve the fit, however slightly.

Figure 3.1- 3.4 illustrate how decisions were made regarding the specific number of peaks used in fitting each spectrum. Whenever possible (i.e., when values of χ^2 less than 10 could be maintained), a minimum number of constraints was used for fitting. Most of the peak parameters (such as isomer shift, quadrupole splitting, and width) were not fixed. They were only held constant if the values, when left unfixed, became unfeasible; that is, they went outside the range of physically possible parameters, as illustrated in Figure 2.6.

More specifically, the majority of the spectra were fit starting with the same input parameters. These parameters included three doublets, one with an isomer shift at 0.39 mm/s and a quadrupole splitting between 1.20 and 1.30 mm/s, a second doublet with an isomer shift at 0.38 mm/s and a quadrupole splitting between 1.0 mm/s and 1.2 mm/s, and the third with an isomer shift around 0.41 mm/s and a quadrupole splitting between 0.60 mm/s and 0.90 mm/s. These were the basic input doublets; there were some spectra that were slightly different, but they still seemed to fit the general formula. The fourth doublet, when used, was very similar in position to the third doublet, indicating that iron was probably in

the same site in the mineral structure. The sextet, when used, had starting parameters with a hyperfine field in the low 500s T; its quadrupole splitting and isomer shift never stayed the same. The area was always below 14% so the width had to be constrained or it had a tendency to become unreal in width, i.e., below the known linewidth for Fe, which is roughly 0.19 mm/s.

Figure 3.1: Jarosite 6 fit with one doublet



To illustrate the fitting process, jarosite 6, which has a formula of $(\text{H}_3\text{O})_{.32}\text{Na}_{.01}\text{K}_{.67}\text{Fe}_3(\text{SO}_4)_2(\text{OH})_6$, is shown in Figure 3.1 fit with only one doublet. While the doublet has the parameters of the typical jarosite doublet (Table 2.6), with an isomer shift of 0.39 mm/s and a quadrupole splitting of 1.21 mm/s, by inspection it is clear that one doublet alone is not enough to fit the spectrum. This

is easy to see around -0.7 and 1.3 mm/s, where the doublet is too wide on the outside and too narrow in its middle.

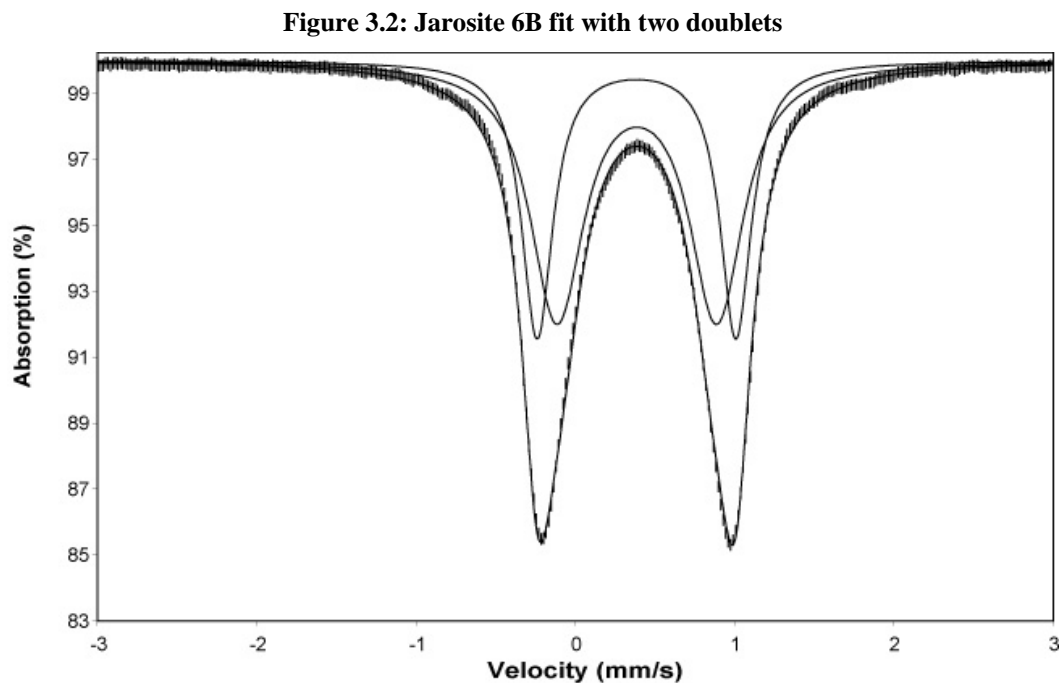


Figure 3.2 illustrates the jarosite 6 fit with two doublets. While this fit is better than the one seen in Figure 3.1, it still has the same problems; it is too wide on the outside near the 100% absorption line and slightly too narrow on the inside. This is hard to see in this figure due to its smallness; the total fit line is very close to the actual spectra. However it runs through the outside edges of the error bars and not through the middle of them. While there are some problems with the fit as evidenced by the fact that the χ^2 is 14, it is still much better than Figure 3.1.

The fit with three doublets is the best so far, as seen in Figure 3.3. The χ^2 is numerically and visually much better than in the previous two fits. The fit now

consists of the typical jarosite peak with $QS = 1.20$ mm/s, (see Table 2.6), one doublet that is slightly smaller, with an isomer shift of 0.38 mm/s and a quadrupole splitting of 1.06 mm/s, and an even smaller one with an isomer shift of 0.40 mm/s and a quadrupole splitting of 0.81 mm/s. Resolution of three sub-components of Fe on the same site in the jarosite structure has not previously been reported in the literature, for reasons to be discussed in later chapters of this thesis. The only problem with this fit is that the sextet isn't fit and can be just barely seen on the inner edges of the wings (e.g., around -1.00 and 1.70 mm/s)

Figure 3.3: Jarosite 6B fit with three doublets

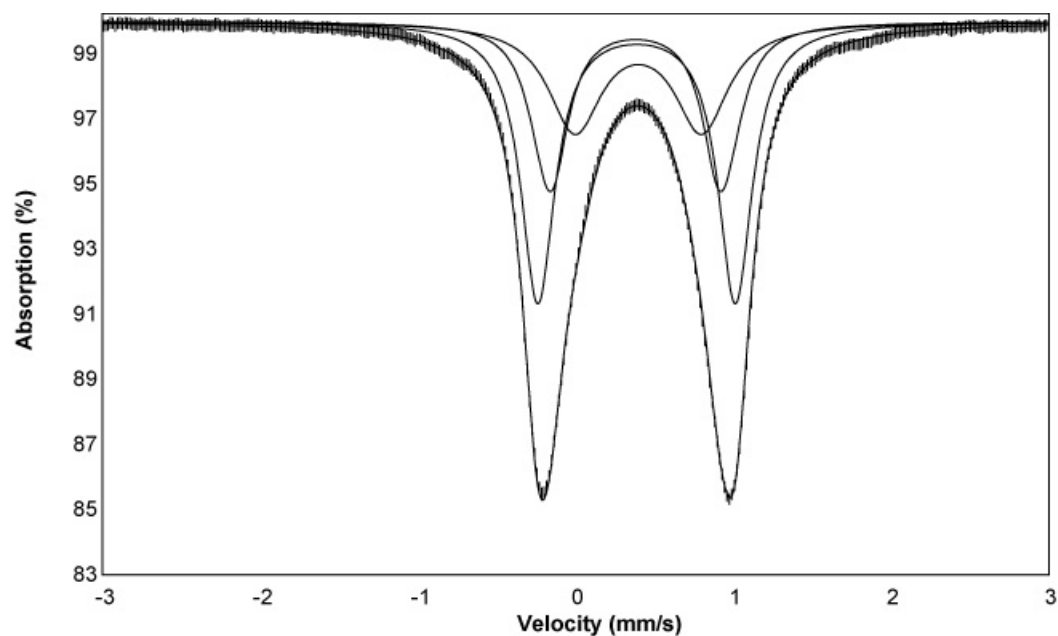
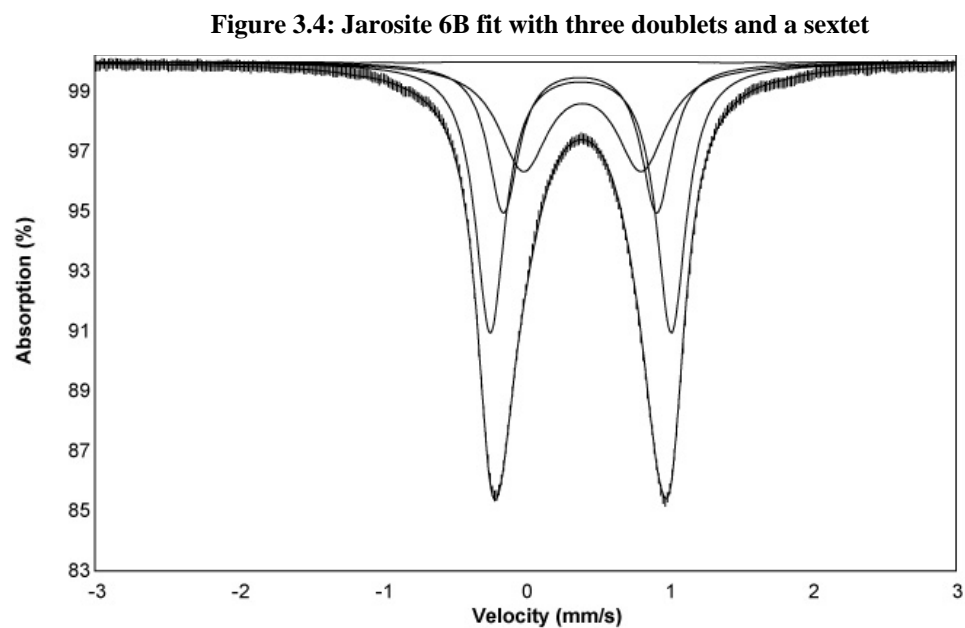


Figure 3.4 is the final version, with three doublets and one sextet. The doublets are almost exactly the same to the ones in Figure 3.3, but the sextet, even though it only has an area of 2.1%, allows the wings as well as the peaks to fit within the error bars.



RESULTS and DISCUSSION

Mössbauer

The room temperature jarosite spectra were generally fit with three doublets and one sextet. However the sextet is not included in the following analysis as its area is very small and therefore not useful for identification. The main area of each spectrum is therefore found in three ferric doublets listed in Table 4.1.

The first doublet has an isomer shift of 0.38 - 0.40 mm/s and a quadrupole splitting of 1.21 – 1.29 mm/s. The area for this doublet varies from 17 – 91 %. This doublet is typically reported as seen in Table 2.9. This is the peak reported by Klingelhöfer et al. (2004) to represent jarosite in the Mars Mössbauer data, because it has the highest quadrupole splitting that a ferric doublet can have and is therefore distinctive. However, many minerals may have the same type of site for the Fe³⁺ (an oxygen octahedron with adjacent SO₄ tetrahedron), such as szomolnokite, and therefore also have the same high quadrupole splitting value for ferric iron.

The second doublet has a larger isomer shift range than the previous doublet, with $\delta = 0.35 - 0.39$ mm/s, though the majority of the values are 0.37 - 0.39 mm/s, which is very similar to the first doublet's values. The $\Delta = 1.02 -$

1.08 mm/s is slightly smaller than the main doublet's values. Its area varies, from 4 – 63%.

The third doublet has a $\delta = 0.39 - 0.30$ mm/s, with the exceptions of $\delta = 0.20$ mm/s at the composition of $(K_{.86}Na_{.04}(H_3O)_{.10})$, and $\delta = 0.48$ mm/s for the compositions of $(K_{.74}Na_{.02}(H_3O)_{.24})$, $(K_{.60}Na_{.07}(H_3O)_{.34})$, and $(K_{.02}Na_{.72}(H_3O)_{.27})$. The $\Delta = 0.47 - 0.94$ mm/s, with the majority being in the middle somewhere. Its area is between 4 – 34%. The third doublet is always present in the spectra, though it doesn't vary systematically with any compositional change. The majority of the area in the spectra seems to fall mostly in the first doublet with the two secondary doublets making up the remaining area.

Table 4.3: Mössbauer table of the two typical jarosite doublets

Formula with Fe ₉ (SO ₄) ₆ (OH) ₁₈	δ(mm/s)	Δ (mm/s)	Area	δ (mm/s)	Δ (mm/s)	Area
(K _{.86} Na _{.04} (H ₃ O) _{.10})	0.39	1.28	84	0.35	1.05	12
	0.38	1.29	91	0.38	1.02	4
(K _{.74} Na _{.02} (H ₃ O) _{.24})	0.38	1.29	82	0.37	1.07	8
	0.39	1.29	54	0.38	1.05	31
(K _{.74} Na _{.01} (H ₃ O) _{.25})	0.40	1.21	20	0.38	1.03	63
	0.40	1.23	17	0.39	1.02	53
(K _{.70} Na _{.01} (H ₃ O) _{.29})	0.39	1.26	52	0.38	1.07	31
	0.39	1.26	56	0.38	1.06	33
(K _{.67} Na _{.01} (H ₃ O) _{.29})	0.39	1.26	45	0.38	1.07	21
	0.39	1.26	47	0.39	1.06	32
(K _{.60} Na _{.07} (H ₃ O) _{.34})	0.39	1.26	75	0.37	1.04	11
	0.39	1.27	48	0.38	1.04	23
(K _{.57} Na _{.10} (H ₃ O) _{.33})	0.39	1.27	68	0.37	1.05	11
	0.39	1.27	55	0.39	1.02	22
(K _{.56} Na _{.02} (H ₃ O) _{.42})	0.39	1.27	41	0.38	1.03	13
	0.39	1.27	57	0.38	1.03	14
(K _{.55} Na _{.03} (H ₃ O) _{.42})	0.39	1.24	51	0.38	1.02	25
(K _{.49} Na _{.16} (H ₃ O) _{.35})	0.39	1.25	25	0.38	1.06	32
(K _{.47} Na _{.02} (H ₃ O) _{.51})	0.39	1.23	19	0.39	1.02	36
(K _{.04} Na _{.68} (H ₃ O) _{.28})	0.39	1.22	19	0.39	1.03	46
(K _{.03} Na _{.78} (H ₃ O) _{.19})	0.39	1.27	49	0.38	1.07	36
(K _{.02} Na _{.72} (H ₃ O) _{.27})	0.39	1.23	60	0.38	1.07	32
(K _{.01} Na _{.65} (H ₃ O) _{.34})	0.39	1.27	33	0.39	1.08	34
(K _{.01} Na _{.83} (H ₃ O) _{.16})	0.39	1.25	32	0.38	1.07	45
(Na _{.83} (H ₃ O) _{.17})	0.39	1.23	27	0.38	1.04	48

The Mössbauer results are shown in a graphical format in Figure 4.1. A, B, and C show the variation of isomer shift with composition. Only the first two doublets are being shown in the figure because the third doublet has a large range and no clear trends. Isomer shift seems to decrease with the percent potassium in the sample in both doublets and increase slightly with an increase of sodium in the

sample in both doublets. While the percent hydronium in the sample increases, in both the H₃O-Na series, the solid data points, and the K-H₃O series, though there is more of an increase in the second doublet than the first. It is important to note that while there are trends, they occur over a very narrow range.

In parts D, E, and F of Figure 4.1, the quadrupole splitting is plotted against composition. The quadrupole splitting seems to increase with the percentage of K in both doublets, though the trend is more obvious in the first doublet. There seems to be a decrease with the percentage of Na versus quadrupole splitting in the first doublet, and stays constant with the percentage of Na in the second doublet. The quadrupole splitting stays constant with the percent of H₃O in the first doublet and decrease with the percentage of H₃O in the sample.

Figure 4.1: Graphs illustrating the isomer shift and quadrupole splitting in variation due to compositional change in the first and second doublet

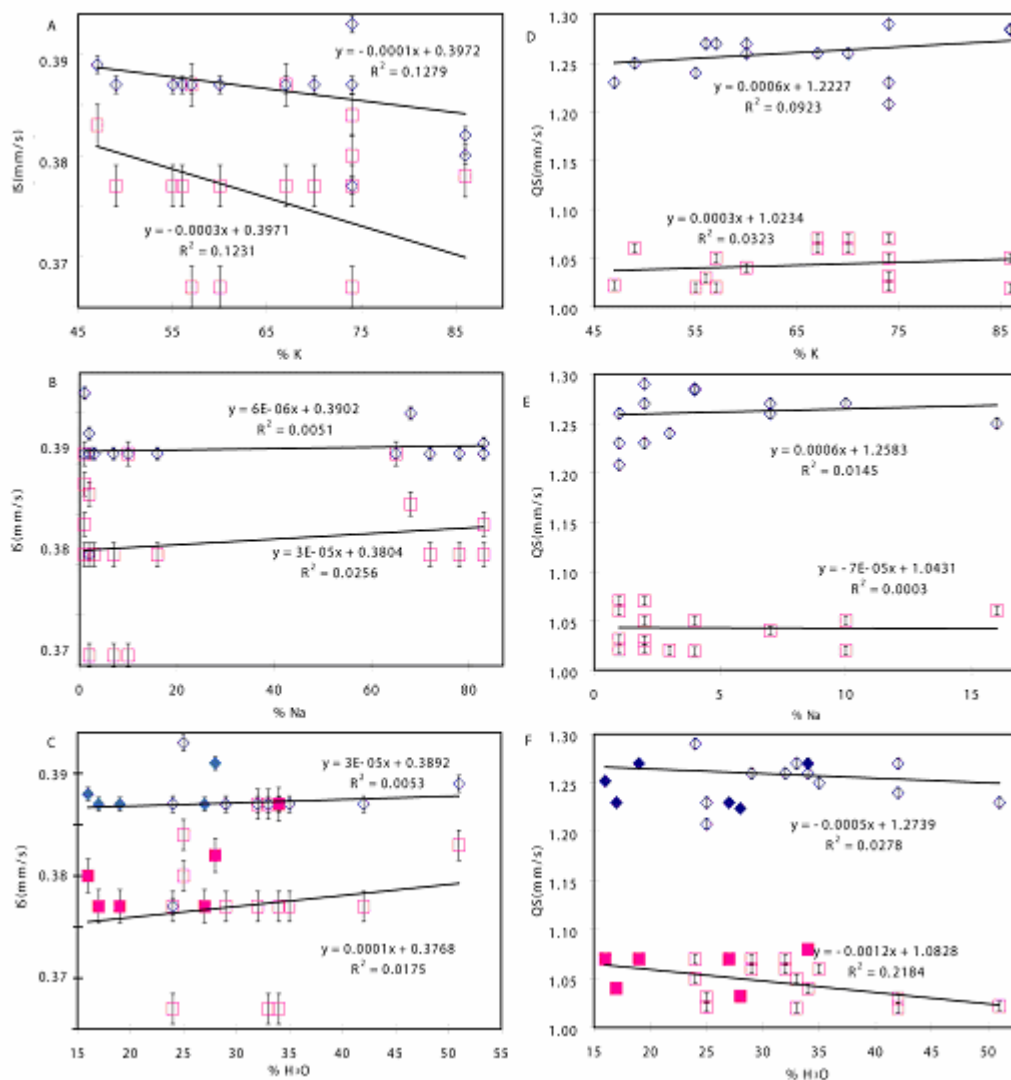


Figure 4.2: Graphs comparing Mössbauer jarosite data from this study to previous work

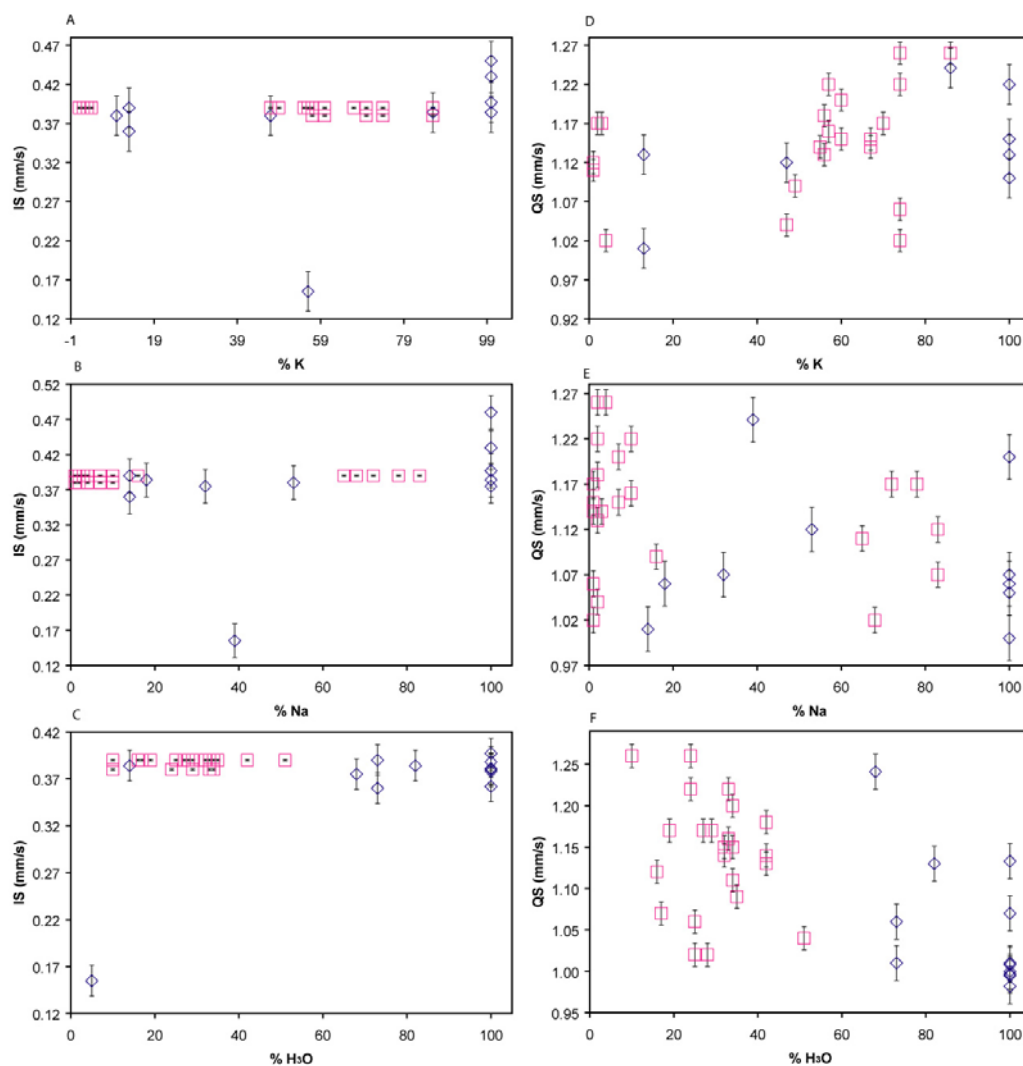


Figure 4.2 has graphs showing all the previously published Mössbauer data from the literature, shown as blue diamonds, along with data from the current study, shown as pink squares. The left displays isomer shift versus composition and the quadrupole splitting versus composition is on the right side. The vast majority of previous studies of jarosite did not give chemical compositions for

their samples, most were a percentage of another more complex larger sample, and therefore just called identified by general formula for jarosite. There were a few that were listed with a formula and those are represented in Figure 4.2 (Grinkevich A.Z. et al., 1963, Herzenberg, C.L., et al. 1966, Johnston, 1977, Leclerc, A. 1980, Seymour, K., et al., 1993, Music, S., et al., 1994., and Herbert, R.B., Jr., 1997). This study is the first to examine an entire suite of jarosite samples to determine how composition effects Mössbauer parameters and therefore has the ability to give greater information because it is now possible to compare the composition of jarosite with the fitted parameters.

The previous studies used only one doublet in their published fits, as opposed to the three doublet fits in this study. As is seen in the top graph of Figure 4.2, this study's samples seem to match up fairly well with the majority of values from previous studies, though there are some higher values from previous studies in the upper 0.40 mm/s range. The bottom graph shows that the current study's values for quadrupole splitting are slightly higher than those reported in the previous studies.

To facilitate better comparison with the data from previous studies, all spectra from the current study were fit with only one doublet and these data were used in Figure 4.2. These data are shown in Table 4.2. With only one doublet,

the variation in parameters is much greater than when fit with three doublets. The isomer shift varies from 0.38 – 0.39 mm/s and the quadrupole splitting varies from 1.02 – 1.26 mm/s. The area stays the same because there was only one peak so the area was only 100%.

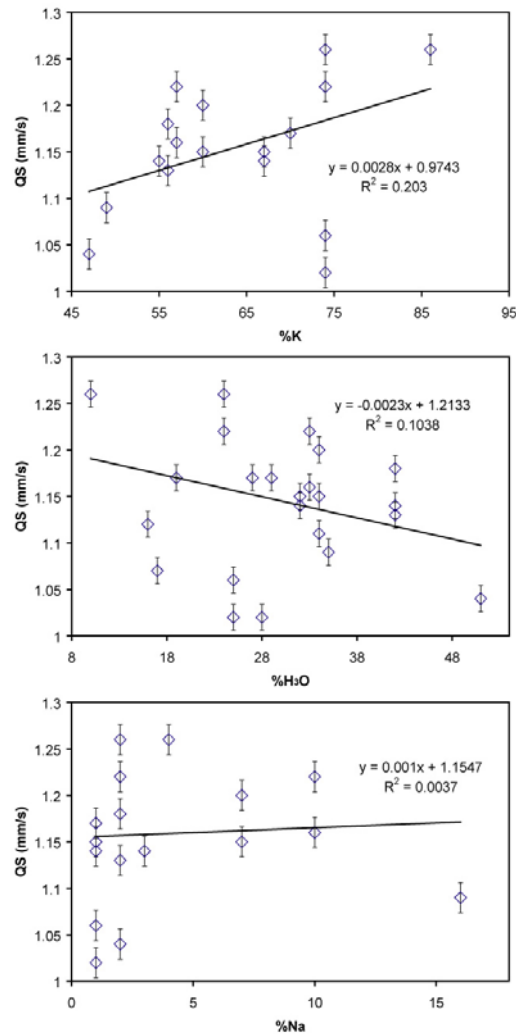
Table 4.4: Mössbauer data for jarosite spectra fit with only one peak

Formula with $\text{Fe}_9(\text{SO}_4)_6(\text{OH})_{18}$	δ	Δ	Area
$(\text{K}_{.86}\text{Na}_{.04}(\text{H}_3\text{O})_{.10})$	0.39	1.26	100.0
$(\text{K}_{.86}\text{Na}_{.04}(\text{H}_3\text{O})_{.10})$	0.38	1.26	100.0
$(\text{K}_{.74}\text{Na}_{.02}(\text{H}_3\text{O})_{.24})$	0.38	1.26	100.0
$(\text{K}_{.74}\text{Na}_{.02}(\text{H}_3\text{O})_{.24})$	0.38	1.22	100.0
$(\text{K}_{.74}\text{Na}_{.01}(\text{H}_3\text{O})_{.25})$	0.39	1.06	100.0
$(\text{K}_{.74}\text{Na}_{.01}(\text{H}_3\text{O})_{.25})$	0.39	1.02	100.0
$(\text{K}_{.70}\text{Na}_{.01}(\text{H}_3\text{O})_{.29})$	0.38	1.17	100.0
$(\text{K}_{.70}\text{Na}_{.01}(\text{H}_3\text{O})_{.29})$	0.39	1.17	100.0
$(\text{K}_{.67}\text{Na}_{.01}(\text{H}_3\text{O})_{.29})$	0.39	1.15	100.0
$(\text{K}_{.67}\text{Na}_{.01}(\text{H}_3\text{O})_{.29})$	0.39	1.14	100.0
$(\text{K}_{.60}\text{Na}_{.07}(\text{H}_3\text{O})_{.34})$	0.38	1.20	100.0
$(\text{K}_{.60}\text{Na}_{.07}(\text{H}_3\text{O})_{.34})$	0.39	1.15	100.0
$(\text{K}_{.57}\text{Na}_{.10}(\text{H}_3\text{O})_{.33})$	0.38	1.22	100.0
$(\text{K}_{.57}\text{Na}_{.10}(\text{H}_3\text{O})_{.33})$	0.39	1.16	100.0
$(\text{K}_{.56}\text{Na}_{.02}(\text{H}_3\text{O})_{.42})$	0.39	1.13	100.0
$(\text{K}_{.56}\text{Na}_{.02}(\text{H}_3\text{O})_{.42})$	0.39	1.18	100.0
$(\text{K}_{.55}\text{Na}_{.03}(\text{H}_3\text{O})_{.42})$	0.39	1.14	100.0
$(\text{K}_{.49}\text{Na}_{.16}(\text{H}_3\text{O})_{.35})$	0.39	1.09	100.0
$(\text{K}_{.47}\text{Na}_{.02}(\text{H}_3\text{O})_{.51})$	0.39	1.04	100.0
$(\text{K}_{.04}\text{Na}_{.68}(\text{H}_3\text{O})_{.28})$	0.39	1.02	100.0
$(\text{K}_{.03}\text{Na}_{.78}(\text{H}_3\text{O})_{.19})$	0.39	1.17	100.0
$(\text{K}_{.02}\text{Na}_{.72}(\text{H}_3\text{O})_{.27})$	0.39	1.17	100.0
$(\text{K}_{.01}\text{Na}_{.65}(\text{H}_3\text{O})_{.34})$	0.39	1.11	100.0
$(\text{K}_{.01}\text{Na}_{.83}(\text{H}_3\text{O})_{.16})$	0.39	1.12	100.0
$(\text{Na}_{.83}(\text{H}_3\text{O})_{.17})$	0.39	1.07	100.0

Figure 4.3 shows the trends of the one doublet fits of the Mössbauer parameters versus composition. The quadrupole splitting seems to vary

compositionally; it increases with the % K, decreases with %H₃O, and increases slightly with the % Na. This is similar to the main doublet in the three doublet fit. The graph of the quadrupole splitting versus composition for one doublet fits is somewhat less clear than the analogous graph from the three peak fit (Figure 4.1), especially for the %Na. This could be because the quadrupole splitting decreased with % Na in the main peak and increased with the % Na in the secondary peak, so the combination of the two looks like a flat trend. There are no figures for isomer shift, because as in the previous fits, there is no change due to compositional differences.

Figure 4.3: One doublet fit of quadrupole splitting versus percent composition

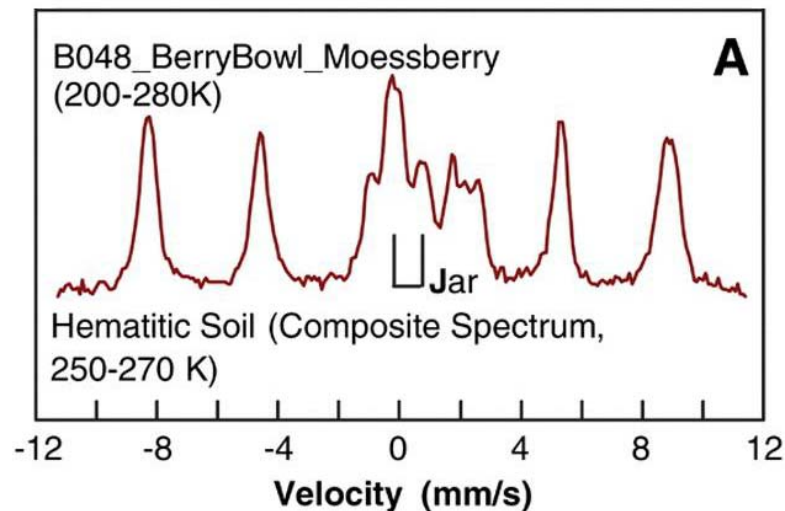


Using the one doublet fits, it is possible to compare this study's results to the Mars Rover Mössbauer science team's results. It was concluded by Klingelhöfer et al. (2004) that jarosite was present in the spectra from the Opportunity rover. The paper gave values only for two of the jarosite doublets, one from an average outcrop matrix, and one from B048. The parameters for both spectra were the same, with an isomer shift of 0.39 mm/s and a quadrupole

splitting of 1.22 mm/s. Jarosite was also reported in several other MER spectra, though specific parameters were not specified.

In this study, the MER spectra in which the jarosite doublet was reported were fit using our methods in order to provide a direct comparison between our parameters and theirs. Table 4.3 shows the jarosite peak fits and the area of the peaks as fit in the Klingelhöfer et al. (2004) paper. Figure 4.4 shows a MER Mössbauer fit with a jarosite assigned doublet.

Figure 4.4: Klingelhöfer et al. (2004) figure of MER Mössbauer data with identified jarosite peak



The doublet is only one of several because the MER data is obtained from rocks which contain more than one mineral. The isomer shift of our fits have values of 0.32 – 0.37 mm/s, with only one outer value at 0.41 mm/s, which are consistent with the Klingelhöfer et al. (2004) value of 0.39 mm/s. Our fits have

quadrupole splitting values of 1.20 – 1.25 mm/s, so the Klingelhöfer et al. (2004) value of 1.22 mm/s fits in perfectly. The areas from this study's fits versus those from the Klingelhöfer et al. study are very similar for the most part. This study has area values from 15-40% and Klingelhöfer et al. study has values from 20-36%.

Table 4.5: The refit Mars Mössbauer data's possible jarosite peak

MER spectra	δ (mm/s)	Δ (mm/s)	Area (%)	Area (Klingelhöfer et al. 2004) (%)
B016	0.36	1.23	29	27
B030	0.35	1.23	25	25
B032	0.41	1.24	29	27
B035	0.32	1.22	40	36
B039	0.37	1.23	16	29
B045	0.36	1.24	23	22
B046	0.37	1.24	21	31
B049	0.36	1.24	22	20
B051	0.35	1.25	15	22
B085	0.34	1.20	35	33

Table 4.4 shows the parameters of $(K_{.74}Na_{.02}(H_3O)_{.24})$ jarosite from 120 – 295K. Low temperature spectra were needed because the MER spectra were obtained at lower than room temperature, between 210 and 270 K, which is the surface temperature of Mars. The main jarosite peak was found to have an isomer shift starting at 0.38 mm/s and increasing to 0.45 mm/s, indicating that isomer shift increases with colder temperatures. The quadrupole splitting has values of 1.29 – 1.30 mm/s, which points to the fact that quadrupole splitting doesn't depend on temperature.

Table 6.4: Low temperature jarosite Mössbauer parameters

	120K	145K	170K	195K	220K	245K	270K	295K
M.F.	506.4	510.1	523.6	521.3	519.7	473.6		528
Γ	0.30	0.30	0.30	0.25	0.25	0.25		0.25
δ	0.53	0.51	0.76	0.59	0.77	-0.01		0.09
Δ	0.48	0.56	1.03	0.80	1.21	-0.79		-0.80
Area	5	6	6	3	5	3		4
Γ	0.34	0.35	0.35	0.33	0.32	0.34	0.33	0.26
δ	0.45	0.40	0.40	0.40	0.40	0.40	0.40	0.38
Δ	1.29	1.30	1.30	1.30	1.30	1.30	1.30	1.29
Area	87	87	85	79	78	79	81	82
Γ	0.25	0.3	0.3	0.3	0.25	0.25	0.89	0.25
δ	0.30	0.29	0.29	0.29	0.25	0.31	0.42	0.37
Δ	1.12	1.11	1.12	1.11	1.04	0.97	1.10	1.07
Area	2	1	2	2	2	3	19	8
Γ	0.41	0.45	0.50	0.88	0.78	0.87		0.51
δ	0.42	0.44	0.44	0.47	0.48	0.48		0.48
Δ	0.45	0.47	0.47	0.79	0.81	0.75		0.55
Area	6	6	7	15	15	15		6
χ^2	3	4	3	2	2	2	2	4

These values when compared with those in the Klingelhöfer et al. (2004) paper cast doubt on their interpretation that the doublet is jarosite because their values for quadrupole splitting, 1.22 mm/s, are too low. Our own fits of the MER spectra also indicate that the isomer shift and the quadrupole splitting are too low to be jarosite.

Our 220K data (from Table 4.4), which were collected at roughly the midpoint of the temperature range over which the MER data were acquired, have a quadrupole splitting of 1.30 mm/s. Thus, the Mars MER doublet is about 0.10 mm/s too low to be assigned to jarosite. Table 4.5 lists three other sulfates that

are similar to the parameters reported to be jarosite by the Klingelhöfer et al. (2004) paper. These other samples are only single samples and they also have variable composition. While these parameters are at room temperature, it has been shown that between 210 and 270 K the isomer shift and quadrupole splitting aren't altered very much by the temperature change. Of the three minerals listed in table 4.5, all of the isomer shifts are comparable to the Klingelhöfer et al. (2004) paper values, though a little high for the refit values. The quadrupole splitting values for Fe³⁺ in copiapite and szomolnokite are in the range of both the Klingelhöfer et al. (2004) paper and the refit values, while the value for botryogen is slightly on the lower end. This is not to say that one of these minerals is the real answer to the doublet in the MER data, but they are indicative of the fact that most sulfates have values that are similar to the ones reported in the Klingelhöfer et al. (2004) paper and this study's refit values.

Table 4.7: Mössbauer parameters of sulfates at room temperature

	Isomer shift (mm/s)	Quadrupole splitting (mm/s)
Botryogen	0.41	1.18
Copiapite	0.43	1.21
Szomolnokite	0.41	1.21

INFRARED

IR spectra in this study, were run from 900 to 6000 nm, as shown in Figure 4.5, with an additional close up in Figure 4.6. There are bands around 937, 1477, 1924, 2273, 2571, 2706, 2973, 4379, 4671, 4867, 4946, and 5082 nm, as shown in Table 4.6. Previous studies, which included values from 2845 – 54945 nm, assigned $\nu(\text{OH})$ to a value between 2845 and 2985 nm, which is similar to the 2973 nm peak. The other peaks don't match up to any others in the current study, though this is possibly due to the fact that this study and previous studies looked at different ranges in wavelength. The more informative part of the IR data comes from changes in the peak location due to compositional changes.

Figure 4.5: IR spectra from 900 to 6000 nm of all of the jarosite samples

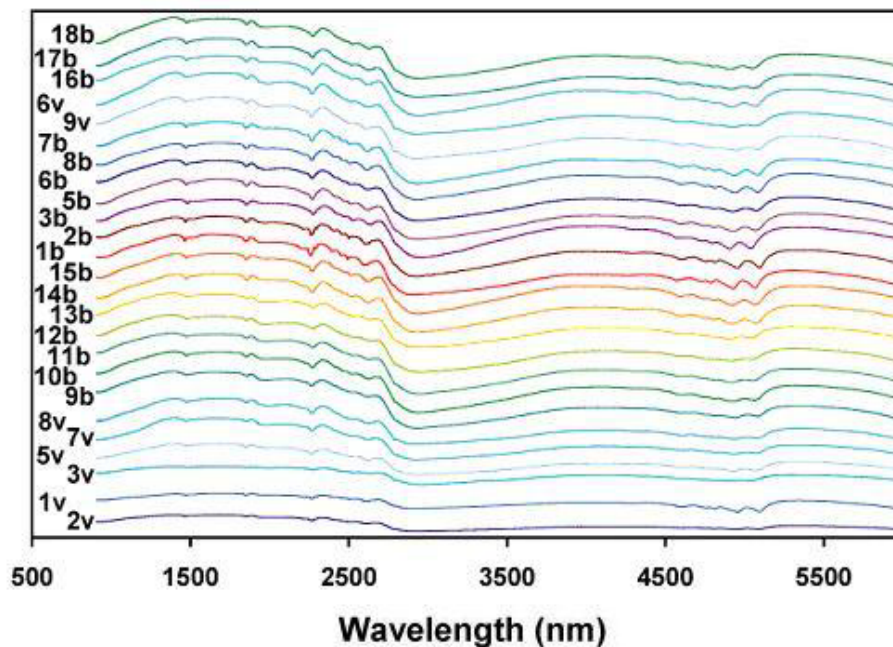


Figure 4.6: Zoomed in IR spectra of all samples from 900 to 2700 nm

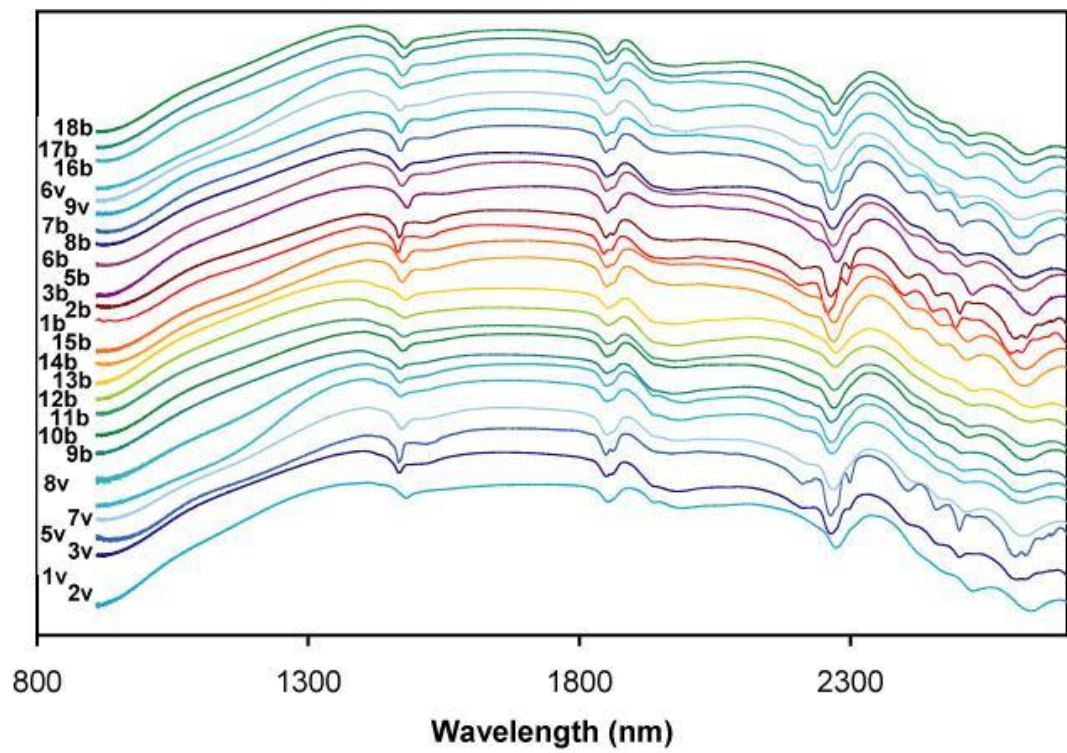


Table 4.6: Jarosite peak values in nm

	Peak Series in nm											
1ba	958	1470	1931	2267	2573	2719	2946	4331	4611	4887	4964	5101
1bc	966	1468	1851	2267	2579	2626	2941	4409	4627	4896	4971	5103
1bb		1468	1932	2267	2574	2719	2946	4403	4709	4896	4896	5078
1v		1470	1970	2267	2579	2627	2953	4324	4605	4885	4962	5098
2b	949	1471	1951	2267	2573	2716	2952	4398	4611	4885	4962	5098
2v		1471	1920	2269	2561	2707	2961	4394	4709	4882	4962	5098
3b	931	1485	1856	2280	2597	2726	2992	4398	4682	4843	4915	5046
3v		1488	1958	2280	2587	2717	2996	4372	4673	4846	4919	5044
5b	944	1477	1955	2274	2573	2721	2978	4403	4613	4859	4943	5083
5vs		1480	1936	2276		2718	2979	4426	4705	4862	4947	5083
6b	939	1477	1918	2273	2565	2709	2970	4385	4690	4864	4957	5093
6vs		1480	1920	2274	2561	2703	2987	4238	4564	4868	4986	5103
7b	945	1474	1951	2272	2569	2717	2956	4341	4609	4866	4947	5088
7v		1476	1916	2274	2558	2701	2994	4362	4688	4871	4957	5093
8b		1473	1960	2272		2719	2963	4394	4709		4952	5093
8v		1475	1920	2270	2559	2710	2968	4388	4705	4873	4962	5093
9b	925	1474	1908	2272	2556	2695	2966	4375	4707	4882	4957	5093
9v		1473	1920	2270	2557	2708	2971	4394	4690	4878	4962	5096
10b	934	1481	1922	2275	2571	2711	2985	4418	4692	4857	4940	5076
11b	926	1485	1911	2277	2569	2700	2983	4396	4686	4857	4936	5068
12b	915	1488	1906	2279	2570	2691	2999	4413	4684	4857	4936	5061
13b	915	1487	1911	2280	2583	2699	2993	4280	4661	4850	4933	5063
14b	944	1477	1970	2274	2573	2724	2974	4407	4701	4857	4940	5081
15b	939	1479	1855	2274	2574	2725	2974	4403	4699	4855	4940	5078
16b	940	1479	1960	2275	2574	2719	2977	4394	4703	4855	4940	5078
17b	927	1481	1918	2275	2571	2711	2980	4394	4699	4855	4936	5073
18b	931	1484	1920	2277	2579	2711	2986	4403	4686	4850	4929	5063

It is important to determine the effect of grain size on the IR spectra outcome. Figure 4.7 shows the same sample run at three different grain sizes, <45 μm , 45-125 μm , and >125 μm . It is interesting to note that the spectra appear to have bands in the same places even if the intensities are slightly different.

Figure 4.7: Shown are three IR spectra of sample 1 taken at different coarsenesses

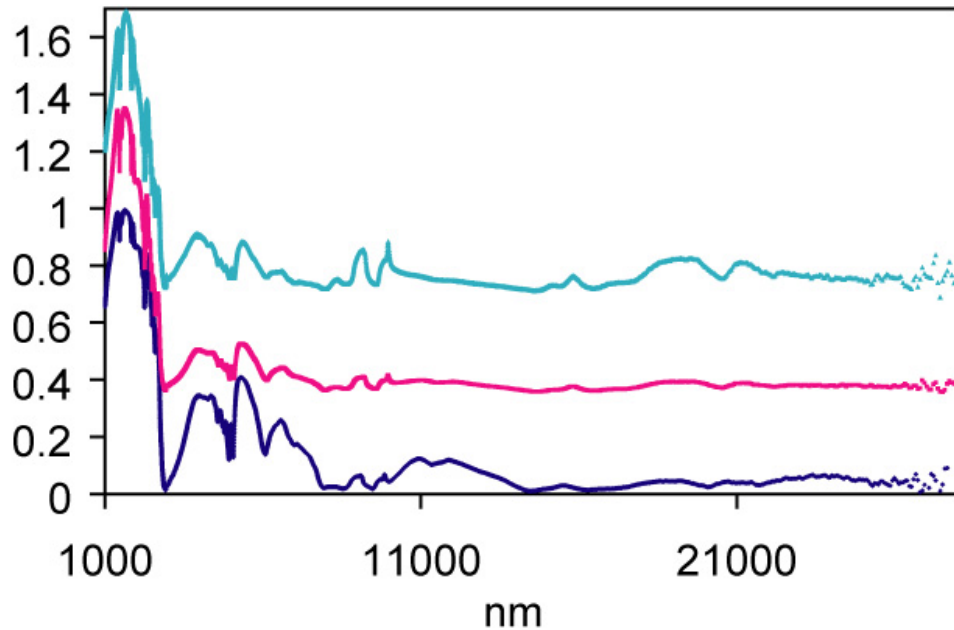
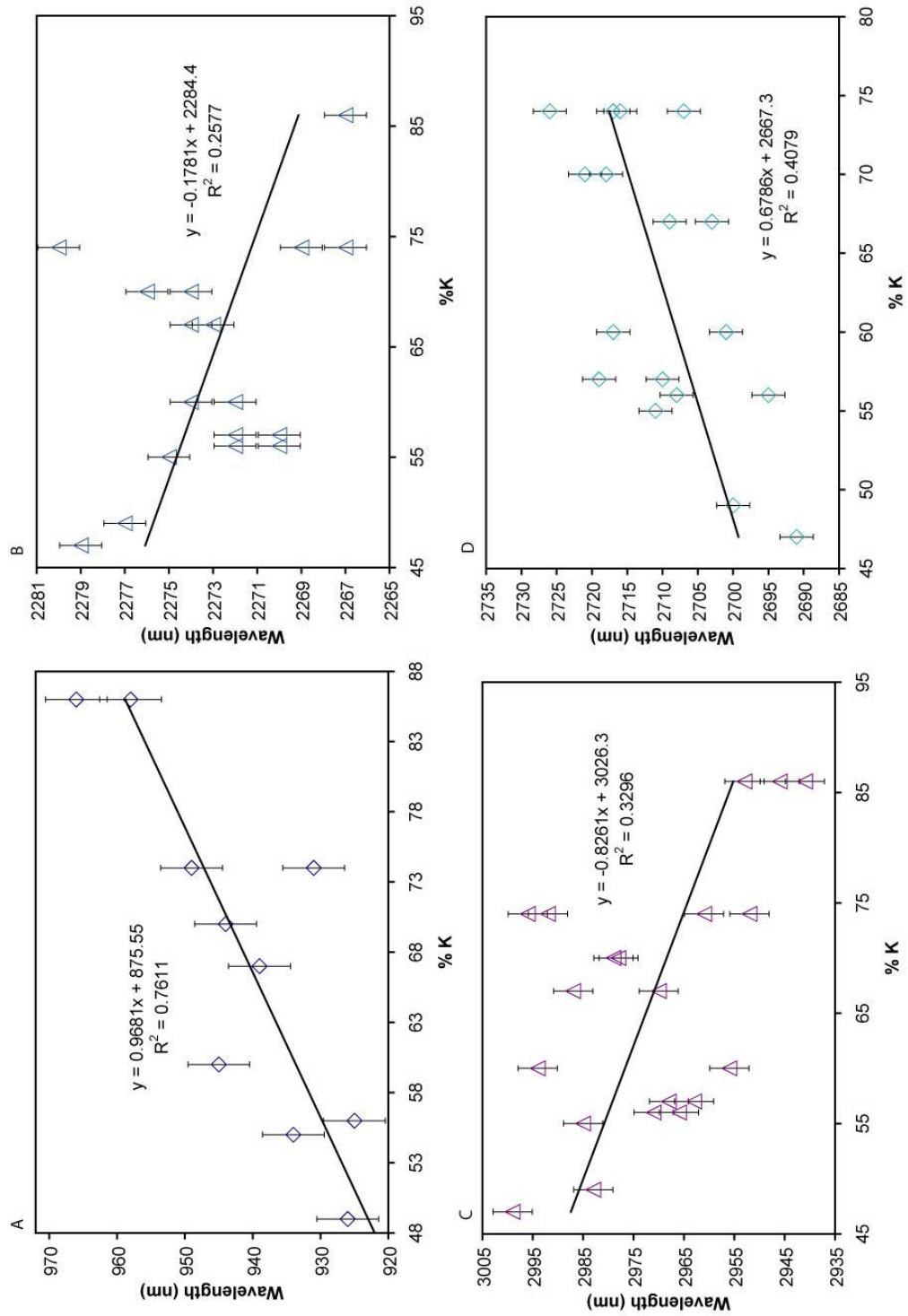


Figure 4.8 shows the changes in composition and the correlating change in the peak position. Four peaks that seem to most clearly indicate the compositional dependence are found at 900, 2200, 2770, and 2980 nm. The peak at 900 nm increases with greater K content. This is very similar to the quadrupole splitting pattern seen in the Mössbauer results. The peak at 2200 nm decreases in wavelength with an increase of K in the sample. At 2770 nm, the wavelength again decreases with a higher percentage of K. The 2980 nm band decreases with the percent K in the sample.

Figure 4.8: Compositional changes in band positions in IR



CONCLUSIONS

The suite of jarosites studied covered samples with variable percentages of potassium, sodium, and hydronium. This made the study a valuable tool for comparing different jarosite compositions. Mössbauer spectroscopy does not have the ability to make definite assignments. However this study has helped to clarify the dependence of the ferric iron in jarosite on the percent composition of potassium and sodium. Mössbauer parameters indicated that the iron was in an oxygen octahedron with adjacent SO_4 tetrahedron, which was already known from the molecular structure of the mineral. The fits also gave clear trends relating the composition of the jarosite to the isomer shift and the quadrupole splitting. The trends indicate that an increase in the percent potassium in the sample causes the sample's isomer shift to decrease, while an increase in sodium and hydronium cause it to increase slightly.

This makes sense as the samples have larger percent potassium when they have lower percent of sodium and hydronium, causing the one to increase when the other decreases. The quadrupole splitting increases with percent potassium, while sodium and hydronium both vary depending on the doublet in question. This correlation means that a higher quadrupole splitting indicates a higher

percentage of potassium and a lower percentage of sodium as well as a lower percentage of hydronium.

The study also included Mössbauer runs at lower temperatures. While the low temperature runs were only using one of the samples in the suite, the data is still useful. It indicates that jarosite has an increasing isomer shift and a steady quadrupole splitting with a lower temperature. As mentioned before, these runs are important for the interpretation of the Mars rover data. Also important for the interpretation of the Mars data is the one peak fits. The quadrupole splitting follows the same changes that it did with three peaks.

The Mars Mössbauer data as reported by the Klingelhöfer et al. (2004) paper indicates the proper value for isomer shift, but the quadrupole splitting is too low to be jarosite, especially considering the fact that this study's refits of the same spectra are in the same range as the original fits. However many sulfates have similar Mössbauer parameters to jarosite. The closest options are copiapite and szomolnokite. It is clear that the peak in the MER data is a sulfate, though which one exactly cannot be definitely stated. What is important is that the assignment of jarosite is probably wrong.

The IR data in this study has the band indicating of the stretching of OH band in common with the previous studies. The other studies had every other band out of the wavelength range that this study examined. There were noticeable band shifts in shifts around 900, 2200, 2770, and 2980 nm. These help to indicate that composition has an effect on the peak position in the IR spectra as well as the Mössbauer.

The IR and Mössbauer results both point to the fact that jarosite has slightly different parameters and peak values depending on its composition. From this study it is only possible to draw conclusions about the certain mineralogical variables that were tested however it is interesting to note that all parameters were affected in some way by the changing percentages in the samples. Using this knowledge of how compositional variables affects quadrupole splitting and isomer shift in Mössbauer spectroscopy and band position in IR spectroscopy, it is possible to make more definite jarosite assignments in planetary spectroscopy, especially with spectroscopic data from more than one spectrometer.

This is important for remote and in situ planetary exploration because the mineral type is rarely definitely known using only one spectrometer and studying a mineral group using two instruments together leads to greater clarification of identification parameters, which leads to more correct identifications. For

example, with the results from this study it would be possible to identify jarosite using these two spectroscopic tools in combination. The Mössbauer parameters have now been shown to include three peaks and the parameters of the three peaks have been quantified. The previous IR studies have already documented the typical jarosite peaks, but this study has shown the correlation between the composition of the sample and the position of the bands. With these data, jarosite identifications and even identifications of the composition of the jarosite may be made with greater certainty.

REFERENCES

- Adler, H. H. and Kerr, P.F. (1965) Variations in Infrared Spectra, Molecular Symmetry and Site Symmetry of Sulfate Minerals. *The American Mineralogist*, 50, 132-147.
- Afanasev, A.M., Gorobchenko, V.D., Kulgawczuk, D.S., and Lukashevich, I.I. (1974). Nuclear γ -Resonance in Tron Sulphates of the Jarosite Group. *Physica status solidi*, 26,697- 701.
- Ahmed, M. A., Vandenberghe, R.E., De Grave, E., Eissa, N.A., and Ibarra, J.V. (1999) Characterisation of Spanish coal by means of Mössbauer spectroscopy. *Fuel*, 78, 453-457.
- Ahmed, M. A., Blesa, M.J., Juan, R., and Vandenberghe, R.E. (2003) Characterisation of an Egyptian coal by Mössbauer and FT-IR spectroscopy. *Fuel*, 82, 1825-1829.
- Allen and Day (1935)
- Audley, G. J., Pyne, G.S., Tricker, M.J., Cranshaw, T.E., and Laundry, B.J. (1986) A New Approach to the Determination of Pyrite in Coals by Mössbauer Spectroscopy. *Fuel*, 65, 1103-1107.
- Barrington, J.L. (1957) The attempted synthesis of an isomorphous series between alunite and jarosite. Honors thesis, Amherst College
- Bell, J.F., Squyres, S.W., Arvidson, R.E., Arneson, H.M., Bass, D., Calvin, W., Farrand, W.H., Goetz, W., Gotombek, M., Greeley, R., Grotzinger, J.,

- Guinness, E., Hayes, A.G., Hubbard, M.Y.H., Herkenhoff, K.E., Johnson, M.J., Johnson, J.R., Joseph, J., Kinch, K.M., Lemmon, M.T., Li, R., Madsen, M.B., Maki, J.N., Malin, M., McCartney, E., McLennan, S., McSween, H.Y., Ming, D.W., Morris, R.V., Dobrea, E.Z.N., Sullivan, R.J., Weitz, C.M., and Wolff, M.J. (2004) Pancam multispectral imaging results from the Opportunity Rover at Meridiani Planum. *Science*, 306, 1703-1709.
- Bishop, J.L., and Murad, E. (2005) The visible and infrared spectral properties of jarosite and alunite. *American Mineralogist*, 90, 1100-1107.
- Brophy, G. P., and Sheridan, M.F. (1965) Sulfate studies IV: The jarosite-natrojarosite- hydronium jarosite solid solution series. *The American Mineralogist*, 50, 1595-1607.
- Burns, R.G. (1987). Ferric Sulfates on Mars. *Journal of Geophysical Research- solid earth and planets*. 92, E570-E574.
- Burns, R.G. (1988) Mössbauer-spectra of planetary materials contributing to visible- near-infrared spectra of regoliths. *Abstracts of papers of the American Chemical Society*, 196.
- Burns, R. G. and Fisher D. S. (1990). Iron-sulfur Mineralogy of Mars: Magmatic Evolution and Chemical Weathering Products. *Journal Of Geophysical Research*, 95, 14,415-14,421.
- Christensen, P.R., Wyatt, M.B., Glotch, T.D., Rogers, A.D., Anwar, S., Arvidson, R.E., Badfield, J.L., Blaney, D.L., Budney, C., Calvin, W.M., Faracaro, A.,

- Ferguson, R.L., Gorelick, N., Graff, T.G., Hamilton, V.E., Hayes, A.G., Johnson, J.R., Knudson, A.T., McSween, H.Y., Mehall, G.L., Mehall, L.K., Moersch, J.Eb., Morris, R.V., Smith, M.D., Squyres, S.W., Ruff, S.W., and Wolff, M.J. (2004) Mineralogy at Meridiani Planum from the Mini-TES experiment on the Opportunity Rover. *Science*, 306, 1733- 1739.
- Dutrizac, J.E., and Jambor, J.L. (2000). Jarosite and their application in hydrometallurgy. In C.N. Alpers, J.L. Jambor, and D.K. Nordstrom, Eds., *Sulfate Minerals: Crystallography, Geochemistry, and Environmental Significance*, 40, 405-452. *Reviews in Mineralogy and Geochemistry*, Mineralogical Society of America, Washington, D.C.
- Eneroeth, E., and Koch, C.B. (2004) Fe-Hydroxysulphates from bacterial Fe²⁺ oxidation. *Hyperfine Interactions*, 156, 423-429.
- Fairchild, J.G. (1933) Artificial jarosite- the separation of potassium from cesium. *American Mineralogist*, 18, 543.
- Fajardo, M., Mojica, J., Barraza, J., Perez Alcazar, G.A., and Tabares, J.A. (1999) Mineral identification in Colombian coals using Mössbauer spectroscopy and X-ray diffraction. *Hyperfine Interactions*, 122, 129-138.
- Gancedo, J. R., Gracia, M., Martinez-Alonso, A., Miranda, J.L., and Tascon, J.M.D. (1992) Mössbauer study of the effect of acidic treatment on iron minerals during the demineralization of coals. *Hyperfine Interactions*, 71, 1403-1406.

- Gracia, M., Gancedo, J.R., Martinez-Alonso, A., and Tascon, J.M.D. (1990) Comparative Mössbauer study of the oxidation of pyrite under different conditions. *Hyperfine Interactions*, 58, 2581-2588.
- Grinkevich, A. Z. and Kul'gavchik., D.S. (1963) The fine structure of Mössbauer spectra in mineral compounds of iron. *Proceedings of the Dubna Conference on the Mössbauer Effect*, 18-EOA.
- Herbert, R. B. J. (1997) Properties of goethite and jarosite precipitated from acidic groundwater, Dalarana, Sweden. *Clays and Clay Minerals*, 45, 261-273.
- Herzenberg, C. L., and Toms, D. (1966). Mössbauer Absorption Measurements in Iron-containing Minerals. *Journal Of Geophysical Research*, 71, 2661-2677.
- Hryniewicz, A.Z., Kubisz, J., and Kulgawczuk, D.S. (1965). Quadrupole splitting of the 14.4 keV gamma line of ^{57}Fe in iron sulphates of the jarosite group. *Journal of Inorganic Nuclear Chemistry*, 27, 2513- 2517.
- Huffman, G. P., and Higgins, F.E. (1978) Mössbauer studies of coal and coke: quantitative phase identification and direct determination of pyritic and iron sulphide sulphur content. *Fuel*, 57, 592-604.
- Huggins, F. E., Huffman, G.P., and Lin, M.C. (1983) Observations on low-temperature oxidation of minerals in bituminous coals. *International Journal of Coal Geology*, 3, 157-182.

- Johnston, J.H. (1977). Jarosite and akagenite from White Island Volcano, New Zealand- an x-ray and Mossbauer study. *Geochimica et Cosmochimica acta*, 41, 4, 539-544.
- Kinoshitea, K. (1955) *Kobutsugaka Zasshi*, 2, 121.
- Klingelhöfer, G., Morris, R.V., Bernhardt, B., Schroder, C., Rodionov, D.S., de Souza, P.A., Yen, A., Gellert, R., Evlanov, E.N., Zubkov, B., Foh, J., Bonnes, U., Kankeleit, E., Gutlich, P., Ming, D.W., Renz, F., Wdowiak, T., Squyres, S.W., and Arvidson, R.E. (2004) Jarosite and hematite at Meridiani Planum from Opportunity's Mössbauer spectrometer. *Science* 306, 1740-1745.
- Komraus, J. L. and P., E.S. (1988) Determination of iron compounds in anthracites and lignites by Mössbauer spectroscopy. *Koks, Smola, Gaz*, 33, 203-207.
- Leclerc, A. (1980) Room temperature Mössbauer analysis of jarosite-type compounds. *Physics and Chemistry of Minerals*, 6, 327-334.
- McSween, H.Y. (1985) SNC meteorites - clues to Martian petrologic evolution. *Review of Geophysics*, 23, 391-416.
- Morris, R. V., Ming, D. W., et al. (1996) An occurrence of jarositic tephra on Mauna Kea, Hawaii; implications for the ferric mineralogy of the Martian surface. *Mineral spectroscopy; a tribute to Roger G. Burns Special Publication - Geochemical Society*, 5, 327-336.

- Musić, S., Orehovec, Z., Popovic, S., and Czako-Nagy, I. (1994) Structural properties of precipitates formed by hydrolysis of Fe^{3+} ions in $\text{Fe}_2(\text{SO}_4)_3$ solutions. *Journal of Materials Science*, 29, 1991-1998.
- Musić, S., Šarić, A., Popović, S., Nomura, K., and Sawada, T. (2000) Forced hydrolysis of Fe^{3+} ion in $\text{NH}_4\text{Fe}(\text{SO}_4)_2$ solution containing urotropin. *Croatica Chemica Acta*, 73, 541-567.
- Parker, R.L. (1954) Alunite alteration at Marysvale, Utah: Ph.D. Dissertation, Columbia University.
- Pax, R.A., and Clark, P.E. (1988) Application of Mössbauer spectroscopy to the coals of central queensland. *Hyperfine Interactions*, 41, 839-842.
- Powers, D. A., Rossman, G.R., Schugar, H.J., and Gray, H.B. (1975) Magnetic behavior and infrared spectra of jarosite, basic iron sulfate, and their chromate analogs. *Journal of Solid State Chemistry* 13, 1-13.
- Reyes, F. A.G., Barraza, J.M., Bohorquez, A., Tabares, J.A., Speziali, N.L. (2003) Mössbauer and XRD characterization of the mineral matter of coal from the Guachinte mine in Colombia. *Hyperfine Interactions*, 148, 39-46.
- Ribeiro, F.R., Mussel, W.N., Fabris, J.D., Novais, R.F., and Garg, V.K. (2003) Identification of iron-bearing minerals in solid residues from industrial kaolin processing. *Hyperfine Interactions*, 148/149, 47-52.

- Ristić, M., Musić, S., and Orehovec, Z. (2005) Thermal decomposition of synthetic ammonium jarosite. *Journal of Molecular Structure*, 744-747, 295-300.
- Rodríguez, N., Menéndez, N., Tornero, J., Amils, R., and de la Fuente, V. (2005) Internal iron biomineralization in *Imperata cylindrical*, a perennial grass: chemical composition, speciation and plant localization. *New Phytologist*, 165, 781-789.
- Ross, S. D. (1974) Sulphates and other oxy-anions of group VI. The infrared spectra of minerals. V. C. Farmern. London, Mineralogical society: 423-444.
- Saito, J. (1962) Report of Geological survey Hok, 28, 1.
- Sasaki, K., Tanaike, O., and Konno, H. (1998) Distinction of jarosite-group compounds by raman spectroscopy. *Canadian Mineralogist*, 36, 1225-1235.
- Serna, C. J., Cortina, C.P., and Ramos, J.V.G. (1986) Infrared and raman study of alunite-jarosite compounds. *Spectrochimica Acta*, 42, 729-734.
- Smith, D.K., Roberts, A.C., Bayliss, P., Liebau, F.(1998) A systematic approach to general and structure-type formula for minerals and other inorganic phases. *American Mineralogist*, 83, 126-132.
- St. Seymour, K., Denes, G., and Townsend, M. (1993). An unusual palagonite from Nisyros Volcano, Aegean Island Arc, Greece. *Neues Jahrbuch fur Mineralogie*, 165, 111-121.

- Takano, M., Shinio, T., Kiyama, M., and Takada, T. (1968). Magnetic Properties of Jarosites, $\text{RFe}_3(\text{OH})_6(\text{SO}_4)_2$ ($\text{R}=\text{NH}_4, \text{Na}$ or K). *Journal of Physical Science of Japan*, 25, 902.
- Taneja, S. P., and Jones, C.H.W. (1984) Magnetic hyperfine parameters of iron containing phases in coal and coal ash. *Nuclear Physics and Solid State Physics Symposium*, 26, 288-289.
- van der Kraan, A. M., Niemantsverdriet, J.W., and Gerkema, E. (1984) Mössbauer spectroscopy used in energy studies. *Energiespectrum*, 84, 104-111.
- Verma, H. C. and Tripathi, R.P. (2000) Characterization of iron-bearing minerals in Giril lignite from Rajasthan and study of their decomposition during combustion using ^{57}Fe Mössbauer spectroscopy. *Fuel*, 79, 599-606.
- Waanders, F. B., E. Vinken, et al. (2003) Iron minerals in coal, weathered coal and coal ash - SEM and Mössbauer results. *Hyperfine Interactions*, 148, 21-29.
- Warshaw, C.M. (1956) The occurrence of jarosite in underclays. *American Mineralogist*, 41, 288-296.
- Wivel, C. and S. Mørup (1981) Improved computational procedure for evaluation of overlapped hyperfine parameter distributions in Mössbauer spectra. *Journal of Physics E: Scientific Instruments*, 14, 605-610.
- Zelenov and Tkachenko (1970)